Ph.D. thesis

# Effect of PARP inhibition on cuprizone-induced pathological changes in a rodent model of multiple sclerosis

**Sára Vető, M.D.**

Department of Biochemistry and Medical Chemistry

Faculty of Medicine

University of Pécs

Ph.D. Program leader: Prof. Balázs Sümegi, Ph.D., D.Sc.

Supervisor: Prof. Ferenc Gallyas Jr., Ph.D., D.Sc.

Pécs

2010

**TABLE OF CONTENTS**

**ABBREVIATIONS**

4HQ: 4-hydroxiquinazoline
AIF: apoptosis inducing factor
BBB: blood-brain barrier
cTEC: cortical thymic epithelial cell
CA II: carbonic anhydrase II
CNS: central nervous system
CPZ: cuprizone
Cyc: CyChrome
DAB: 3,3'-diamino-benzidine
DAPI: 4',6'-diamidino-2-phenylindole
DN: double negative
DP: double positive
EpCAM: epithelial cell adhesion molecule
EAE: experimental autoimmune encephalomyelitis
ERK1/2: extracellular signal-regulated kinase 1/2
FITC: fluorescein isothyocyanate
IL-2: interleukin-2
JNK: c-Jun N-terminal kinase
mTEC: medullary thymic epithelial cell
MAPK: mitogen activated protein kinase
MBP: myelin basic protein
MHC: major histocompatibility complex
MMP-9: matrix metalloproteinase-9
MOMP: mitochondrial outer membrane permeabilization
MR: magnetic resonance
MRI: magnetic resonance imaging
p38: p38 mitogen activated protein kinase
PAR: poly(ADP-ribose)
PARG: poly(ADP-ribose)glycohydrolase
PARP: poly(ADP-ribose) polymerase
PBS: phosphate buffered saline
PE: phycoerythrin
PFA: paraformaldehyde
PI: propidium iodide
PI-3K: phosphatidylinositol-3 kinase
PKB/Akt: protein kinase B/Akt
ROS: reactive oxygen species
SP: single positive
TBS: Tris buffered saline
TCR: T cell receptor
TEC: thymic epithelial cell

# 1. INTRODUCTION

## 1.1 Multiple sclerosis

Multiple sclerosis (MS) is a common, chronic disease of the brain and the spinal cord characterized by a presumed autoimmune inflammation, focal demyelination and axonal degeneration [Noseworthy et al.,2000]. Although immunomodulatory treatments are available to counteract the common inflammatory pathology, no treatments exist to prevent demyelination, which may contribute to axonal degeneration, the best pathological correlate of clinical disability in MS [Naismith and Cross,2005]. Environmental exposure and genetic susceptibility are both implicated as the cause of MS, although disease mechanism and pathogenesis are still under debate [Compston and Coles,2008].

Individuals with MS become symptomatic usually in the third and fourth decade, and the median time to death is around 30 years from disease onset, with a prevalence of between 50:100.000 and 300:100.000 in Europe, North America and Australasia. MS is more common in women than men (F:M ratio~2:1) [Koch-Henriksen and Sorensen,2010]. MS is a heterogeneous disease, clinical manifestations indicate the involvement of motor, sensory, visual and autonomic systems but many other symptoms and signs can occur. Clinical course is also variable, 80% of patients present with relapsing-remitting multiple sclerosis, where with time, recovery from each episode is incomplete and persistent symptoms accumulate. Eventually, around 65% of patients enter the secondary progressive phase; in 20%, the illness is progressive from onset [Compston and Coles,2008].

Moreover, there is profound heterogeneity also in neuroradiological appearance of the lesions, response to therapy and pathological pattern of demyelination. Although all pathological patterns show a T cell- and macrophage-dominated inflammatory reaction, in pattern I it is the macrophage released toxins such as TNF-alpha or reactive oxygen species (ROS), whereas in pattern II it is the antibodies and complement that specifically mediate demyelination. While destruction of myelin develops in association with inflammation, in the earliest lesions of pathological subtypes of pattern III and IV apoptosis-like depletion of oligodendrocytes have been described suggesting degenerative processes [Lucchinetti et al.,2000] (**Fig. 1**). An alternative hypothesis to the heterogeneous pathogenesis of MS even proposes that oligodendrocyte apoptosis represents the first and earliest stage of all lesions

resulting in primary demyelination unmasking tissue antigens and secondary autoimmune inflammation [Barnett and Prineas,2004]. Depletion of oligodendrocytes then occurs progressively during lesion evolution [Frohman et al.,2006].

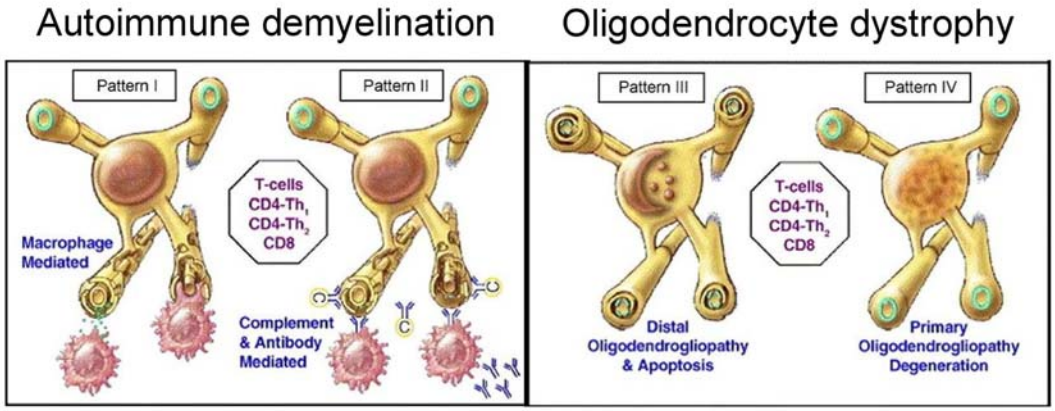


**Fig. 1 Summary of heterogeneous pathogenetic mechanisms involved in the formation of acute multiple sclerosis lesions.** All active lesions occur on a background of an inflammatory process, composed mainly of T lymphocytes and macrophages. Despite the similarities in the inflammatory reaction, the lesions segregate into four patterns of demyelination based on plaque geography, extent and pattern of oligodendrocyte pathology, evidence for immunoglobulin deposition and complement activation, and pattern of myelin protein loss. The four patterns are: pattern I: macrophage-associated demyelination, pattern II: antibody/complement-associated demyelination, pattern III: distal dying-back oligodendrogliopathy, pattern IV: primary oligodendrocyte degeneration. Figure adopted from [Denic et al.,2010].

Recently, mitochondrial dysfunction has been indicated to play a role in loss of oligodendrocytes and axons in MS [Kalman et al.,2007]. Fulminate MS lesions with profound oligodendrocyte apoptosis (pattern III) reveal a pattern of hypoxia-like tissue injury, which seems to be induced by a dysfunction of complex IV of the mitochondrial respiratory chain [Aboul-Enein et al.,2003; Lucchinetti et al.,2000; Mahad et al.,2008]. In such MS lesions, oligodendrocyte apoptosis follows a caspase-independent pathway [Aboul-Enein et al.,2003; Barnett and Prineas,2004].

### 1.2 Animal models of multiple sclerosis

Over the past decades a number of animal models have been developed in order to understand a variety of aspects of human MS. The most extensively studied model is the purely autoimmune experimental autoimmune encephalomyelitis (EAE), induced by the subcutaneous injection of an emulsion that contains an adjuvant and synthetic peptides derived from myelin proteins [Denic et al.,2010; Segal,2003]. Virus-induced demyelination, such as Theiler's murine encephalomyelitis virus

infection models an autoimmune response triggered by viral infection in the central nervous system (CNS). In this model epitope spreading from virus to self epitopes has been observed [Miller et al.,1997; Nelson et al.,2004]. Pattern I and II MS shows similarities to these T-cell plus antibody–mediated or T-cell-mediated autoimmune encephalomyelitis. Pattern III and IV are rather suggestive of a primary oligodendrocyte dystrophy, reminiscent of toxin-induced demyelination such as the cuprizone or lysolecithin models [Lucchinetti et al.,2000].

A non-inflammatory experimental primary demyelination induced by the copper chelator cuprizone in young adult mice results in multi-focal demyelination and apoptosis of oligodendrocytes in particular brain areas, mainly corpus callosum and superior cerebellar peduncle [Matsushima and Morell,2001]. Mitochondrial pathomechanism was assumed since giant mitochondria have been observed in the liver and oligodendrocytes of cuprizone-treated mice [Suzuki and Kikkawa,1969]. Supporting this notion, increased ROS production and decreased activities of the various complexes of the respiratory chain were found in mitochondria of cuprizone-treated oligodendroglia cells [Pasquini et al.,2007]. However, and in contrast to EAE, the number of T cells is negligible in the demyelinated corpus callosum and T cell activation has not been observed in the cuprizone model [Remington et al.,2007].

### 1.3 Roles of poly(ADP-ribose) polymerase

Impaired functioning of the mitochondrial respiratory chain results in excessive production of ROS that induces damage to various cellular components including the DNA [Turrens,2003]. The nuclear enzyme poly(ADP-ribose) polymerase (PARP) functions as a DNA damage sensor and signalling molecule. Activated PARP uses nicotinamide adenine dinucleotide ($NAD^+$) as substrate and forms long branches of ADP-ribose polymers on γ-carboxyl group of glutamic acid residues on a number of nuclear target proteins (heteromodification) including PARP itself (automodification) [Alano et al.,2004].

PARP-1 is the most abundant of several PARP family members, accounting for more than 85% of nuclear PARP activity and is present in all nucleated cells of multicellular animals [Virag and Szabo,2002]. PARP-1 (116 kDa) is a highly conserved enzyme consisting of three domains: the N-terminal DNA-binding domain (42kDa) containing a nuclear localization signal (NLS) and two zinc finger (ZF) motifs that bind single or double-strand breaks in double-stranded DNA leading to activation

of the enzyme; a central automodification domain (16 kDa) containing possible auto-poly(ADP-ribosyl)ation sites and the BRCT (BRCA1 C-terminal) domain that is known to be involved in protein-protein interactions [Callebaut and Mornon,1997]; and a C-terminal catalytic domain (55kDa) that is the most highly conserved region of the PARP-1 molecule [de Murcia et al.,1994] (**Fig. 2**).

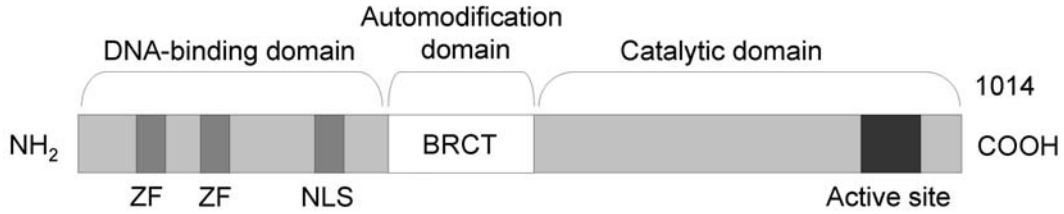


**Fig. 2 Structure of PARP-1.** PARP-1 contains an N-terminal DNA-binding domain, a nuclear localization sequence (NLS), an internal automodification domain, and a C-terminal catalytic domain. The DNA binding domain contains two zing fingers (ZF). The auto-modification domain has a BRCT motif typical of many DNA repair and cell-cycle proteins, and contains phosphorylation sites that regulate PARP-1 activity. Adopted with modification from [de Murcia et al.,1994].

Poly(ADP-ribosyl)ation is involved not only in the detection and repair of DNA damage but plays key roles in many cellular processes, including gene transcription, cell-cycle progression, cell death, chromatin function, and genomic stability [Jagtap and Szabo,2005].

Extensive DNA damage triggers overactivation of PARP eventually resulting in cell dysfunction and death. According to a common hypothesis, overactivation of PARP and (ADP-ribosyl)ation leads to massive utilization of $NAD^+$. Rapid loss of cellular $NAD^+$ and concomitant loss of ATP affects cellular energy metabolism resulting, ultimately, in cell death [Ha and Snyder,2000]. Additionally, PARP activity appears to trigger mitochondrial outer membrane permeabilization (MOMP) and the mitochondria-to-nucleus translocation of apoptosis-inducing factor (AIF) supporting the hypothesis that a nuclear mitochondrial crosstalk dependent on poly(ADP-ribosyl)ation is critical in determining the fate of injured cells [Yu et al.,2002]. Nuclear translocation of AIF mediates chromatin condensation, large-scale fragmentation of DNA and cell death [Susin et al.,1999; Yu et al.,2002]. Each of these events are caspase independent because broad-spectrum caspase inhibitors do not block them [Yu et al.,2002]. The mechanism responsible for PARP dependent release of AIF from mitochondria is to be identified but it might involve PAR signalling [Yu et al.,2006] (**Fig. 3**).

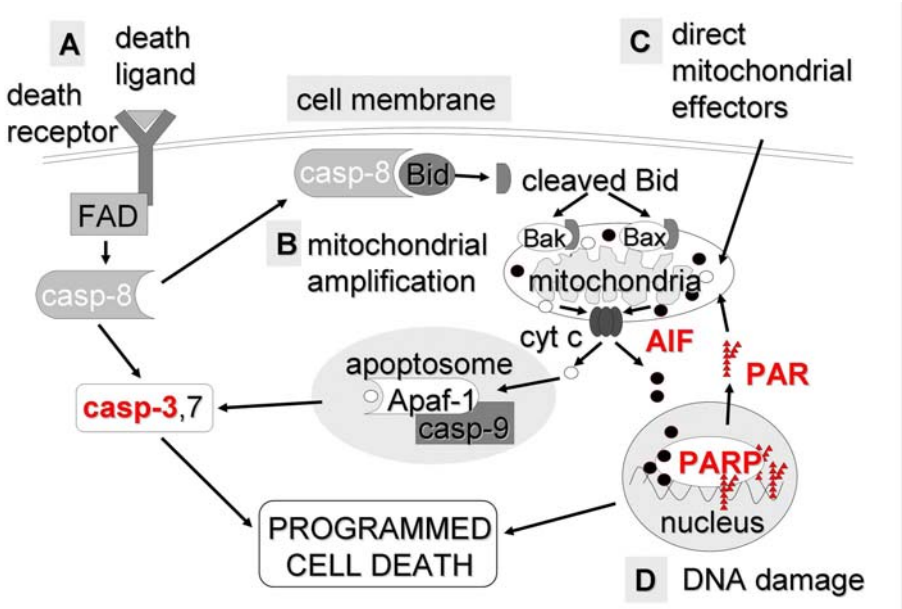


**Fig. 3 Pathways of programmed cell death. A**) Extrinsic, death ligand-receptor triggered pathway executed by caspases. **B**) Death ligand-receptor triggered pathways executed by caspases after a mitochondrial amplification of death signals. **C**) Intrinsic or mitochondrial pathway of cell death triggered by mitochondrial damage and executed by either a mitochondrial mechanism alone or by additional caspase activation. **D**) Cell death triggered by DNA damage induced PARP activation, executed by either a mitochondrial mechanism alone, or by caspase activation. Adopted with modification from [Kalman et al.,2007] and [Hong et al.,2004].

This nuclear mitochondrial crosstalk is supposed to involve PARP-dependent activity modulation of different kinase signalling pathways. One of the major molecules coordinating complex signalling pathways is protein kinase B (PKB), a serine/threonine kinase also known as Akt [Parcellier et al.,2008]. Activated by the insulin/growth factor-phosphatidylinositol 3-kinase (PI-3K) cascade, Akt triggers events that promote cell survival and prevent apoptosis through different mechanisms, one of which is the inhibition of AIF translocation to the nucleus [Kim et al.,2007]. It has been shown that PARP activity attenuates the cytoprotective PI-3K-Akt pathway [Tapodi et al.,2005]. The mitogen activated protein kinase (MAPK) cascades are generally activated in response to mitogenic signals, cytokines and environmental stress, and lead to activation of the members of the MAPK family. Three MAPK subfamilies have been identified in mammalian cells: extracellular signal-regulated kinase 1/2 (ERK 1/2) or p44/42 MAPK, p38 MAP kinase (p38) and c-Jun N-terminal kinase (JNK). These MAPK cascades have been shown to participate in a wide array of cellular functions, such as cell growth, cell differentiation, inflammation and apoptosis. Although many MAPK activating stimuli are proapoptotic

or antiapoptotic, the biological outcome of MAPK activation is highly divergent and appears to be largely dependent on the cell type. It has been suggested that PARP activation leads to JNK activation, which leads, in turn, to mitochondrial depolarization, AIF translocation and cell death [Xu et al.,2006]. Moreover, phosphorylation of PARP by ERK2 seems to be necessary for maximal PARP activation after DNA damage [Kauppinen et al.,2006] and this underlines the importance of MAPK cascades in PARP-mediated cell death.

Furthermore, PARP has been shown to function as a co-activator in the nuclear factor (NF)-κB-mediated transcription regulating the expression of various pro-inflammatory proteins, i.e. inducible nitric oxide synthase (iNOS), matrix metalloproteinase-9 (MMP-9) and other pro-inflammatory cytokines and proteases [Hassa et al.,2003; Mattson,2005; Oliver et al.,1999].

PARP mediated cell death and inflammation has been implicated in the pathogenesis of several CNS diseases [Kauppinen and Swanson,2007]. Inhibition of PARP activity reduced brain injury in ischemia-reperfusion, excitotoxicity, oxidant stress and brain trauma [Endres et al.,1997; LaPlaca et al.,2001; Mandir et al.,2000; Zhang et al.,2000]. It was also able to ameliorate inflammation in EAE, the autoimmune model of multiple sclerosis [Scott et al.,2004].

### 1.4 Other features of the cuprizone model

Besides demyelination and oligodendrocyte loss, administration of cuprizone to weanling male C57BL/6 mice up to six weeks results in formation of hydrocephalus and weight loss of the animals [Matsushima and Morell,2001]. Emerson and co-workers found in SJL mice after two weeks of cuprizone treatment a significant decrease in $CD4^+$ single positive (SP)/$CD8^+$ SP T cell ratio in the blood of the animals [Emerson et al.,2001]. Additionally, in EAE, administration of cuprizone beginning one week prior to the injection of the encephalitogen attenuated disease severity [Emerson et al.,2001]. The mechanism of disease suppression could be related to an inhibition of T-cell function since EAE involves stimulation of T-cell mediated immunity.

### 1.5 T cell maturation

T cells, together with B cells, are the main cellular components of the adaptive immune system. They recognize antigens through their T cell receptors (TCR) in

processed and presented form bound to major histocompatibility complexes (MHC). Helper T cells express CD4 as co-receptor on their cell surface and bind to MHC class II, whereas cytotoxic T cells express CD8 and bind to MHC class I, respectively. Upon activation, cytotoxic T cells ($CD8^+$) eliminate foreign peptide presenting cells (virus infected or transformed cells), helper T cells ($CD4^+$) secrete cytokins that regulate or assist in active immune response.

T cells originate from the common lymphoid progenitor cells in the bone marrow. They migrate as immature precursor T cells via the bloodstream into the thymus – anatomically divided into two main parts, the outer cortex and the inner medulla–, which they populate and go through a series of maturation steps. Mature T cells then migrate to peripheral lymphoid organs to differentiate into effector cells and fulfil their function [Allman et al.,2003] (**Fig. 4**).

Thymocyte developmental stages can readily be defined by the expression of the cell surface receptors. The most immature thymocytes express neither the CD3/TCR complex nor the CD4 or CD8 accessory molecules; they are called double negative (DN) $CD4^-CD8^-$ cells. Maturation progresses with the acquisition of CD4 and CD8 markers, generating $CD4^+CD8^+$ double positive (DP) cells [Boyd and Hugo,1991]. At this stage, TCR genes are completely rearranged and CD3/TCR is expressed at low densities. DP thymocytes move deep into the thymic cortex where they meet self-antigens bound to MHC molecules on the surface of cortical epithelial cells. Only those thymocytes whose TCR bind the MHC/antigen complex with adequate affinity will survive, others die by apoptosis (positive selection). Positive selection also coincides with lineage commitment and DP thymocytes undergo a rigorous selection process and eventually become $CD4^+$ SP or $CD8^+$ SP thymocytes with a slight predominance of $CD4^+$ SP cells, which exhibit MHC class II or MHC class I restriction, respectively [Boyd and Hugo,1991].

Thymocytes that survive positive selection move toward the medulla where they are again presented various not thymic tissue related antigens by medullary epithelial cells, dendritic cells and macrophages. Thymocytes that interact too strongly with the antigen/MHC complex die by apoptosis (negative selection). Negative selection allows the establishment of self-tolerance in the T cell repertoire, promoting apoptosis-mediated deletion of most T cells that might potentially react to self proteins and mature, nonself-reacting SP thymocytes are exported to the periphery as antigenic, naïve helper or cytotoxic T cells [Anderson and Jenkinson,2001].

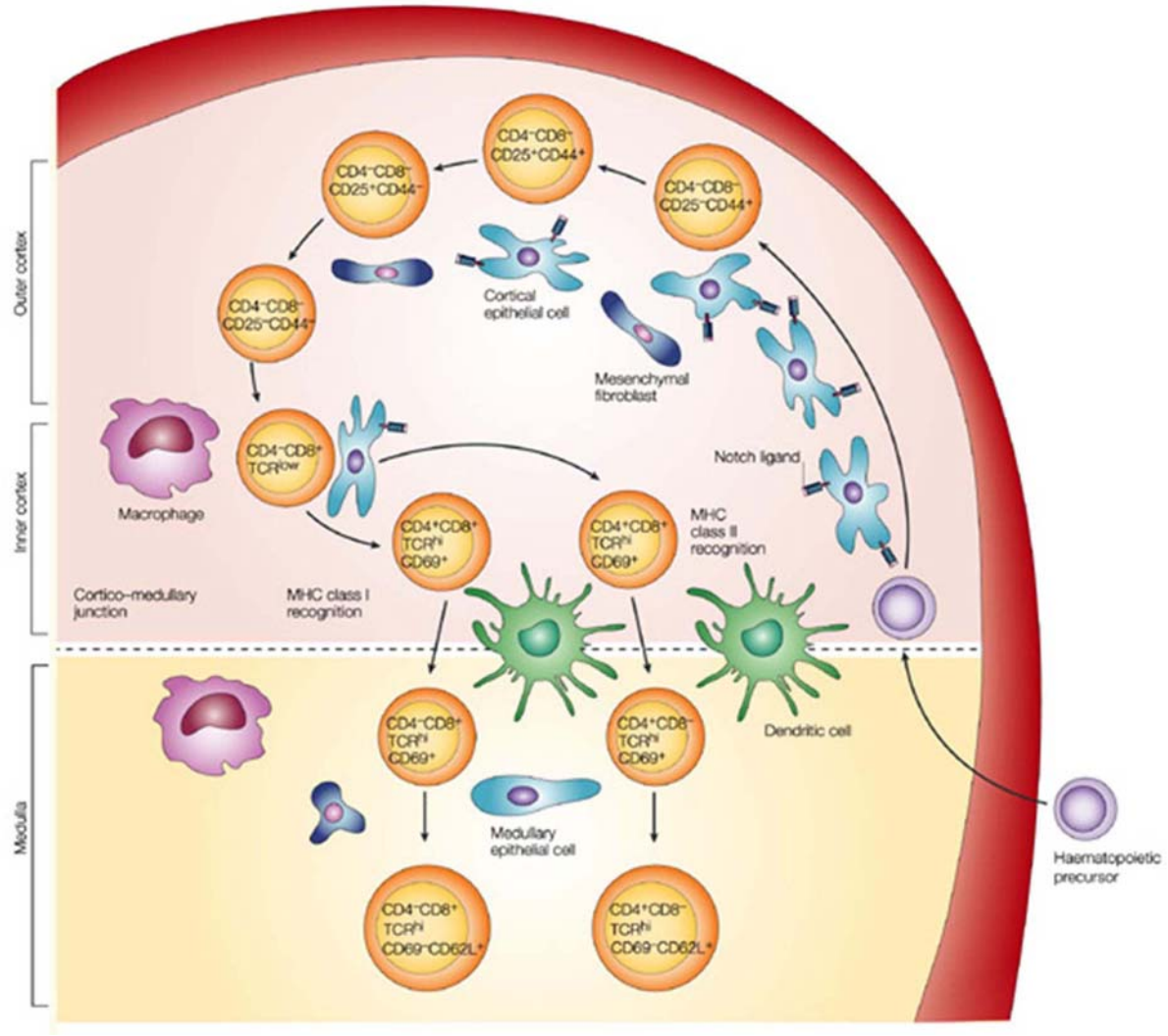


**Fig. 4 Schematic representation of T cell development in the thymus.** The thymic architecture is organized into discrete cortical and medullary areas, each of which is characterized by the presence of particular stromal cell types, as well as thymocyte precursors at defined maturation stages. Thymocyte differentiation is characterized by the expression of well-defined cell-surface markers, including CD4, CD8, as well as the status of the T-cell receptor (TCR). Most immature thymocytes localized in the subcapsular cortical region do not express CD4 or CD8 accessory molecules, nor TCR and are known as double negative (DN, for CD4 and CD8) cells. As they progress in differentiation, they begin to expressTCR as well as CD4 and CD8, becoming double positive (DP) thymocytes, which occupy most of the cortical region. These cells are then submitted to negative and positive selection, moving toward the medulla and becoming single positive (SP) cells for either CD4 or CD8, both expressing high densities of TCR. Adopted from [Zuniga-Pflucker,2004].

### 1.6 Thymic stroma

The thymic stroma provides the molecular and stromal environment for the development of T cells. During maturation thymocytes are intermingled with a

heterogeneous cellular network, the thymic microenvironment composed of thymic epithelial cells (TEC), dendritic cells, macrophages, fibroblasts and extracellular matrix components (**Fig. 4**). In addition to the key antigen presenting interaction, interactions between Notch receptor-expressing thymocytes and thymic stromal cells that express Notch ligand induce the complex programme of T cell maturation [Alves et al.,2009]. Microenvironmental cells modulate thymocyte differentiation by soluble factors comprising cytokins, chemokines and thymic hormones [Anderson et al.,2007; Petrie and Zuniga-Pflucker,2007]. TECs are the major component of the thymic stroma and phenotypically distinct TEC subsets fulfil different functions during T cell development. Therefore, it can be distinguished between cortical epithelial cells (cTEC) mediating commitment, expansion, development of T cell presursors and positive selection in the cortex and medullary epithelial cells (mTEC) playing important role in negative selection mediation and providing survival signals to SP thymocytes. Both mTECs and cTECs express MHC class II and the epithelial cell adhesion molecule (EpCAM) but the two cell types can be distinguished phenotypically on the basis of expression of cortical (majority cytokeratine-$8^+$ and -$18^+$, Ly$51^+$) or medullary (majority cytokeratin-$5^+$ and $14^+$, Ly$51^-$, and by mature mTECs the transcription factor autoimmune regulator (Aire)$^+$) markers [Gray et al.,2006; Klug et al.,2002; Kyewski and Klein,2006]. However, this interaction between thymocytes and thymic epithelial cells is mutual; T cells are required for TEC development and formation of the three dimensional stromal structure. Therefore thymocytes and TECs exist in a dynamic codependence called cross-talk, whereby disruption of thymocyte development impacts on the stroma and vica versa [Anderson and Jenkinson,2001; van Ewijk et al.,2000].

## 2. OBJECTIVES

1. Administration of cuprizone to young adult male mice induces selective oligodendrocyte apoptosis with concomitant demyelination, formation of hydrocephalus and weight loss. Activation of PARP enzyme is involved in cell death processes in many pathological settings and PARP inhibition has been shown to act cytoprotective in many disease models of the CNS. Therefore, our first aim was to investigate, whether PARP is activated upon cuprizone treatment and whether its inhibition has any influence on these known effects of cuprizone.

2. Emerson and co-workers described a disease attenuating effect of cuprizone in EAE, and a decrease in $CD4^+/CD8^+$ T cell ratio of the blood in mice upon two weeks of cuprizone treatment [Emerson et al.,2001]. However, it is not known, whether there are any pathological changes of the thymus in the background of this phenomenon. Accordingly, our aim was to study the effects of cuprizone on thymi of cuprizone-treated mice.

3. Furthermore, the aim of the study was to investigate, whether PARP inhibition can modulate the assumed effect of cuprizone on the thymi of mice.

4. Cuprizone acts as a mitochondrial toxin, leading to impaired mitochondrial functioning and apoptosis of oligodendrocytes. However, the underlying molecular mechanisms of the cell death are not yet known. The aim of the last part of the study was therefore to elucidate the possible mechanisms, signalling pathways involved in oligodendrocyte loss and to investigate the effect of PARP inhibition on these processes.

## 3. MATERIALS AND METHODS

**Cuprizone model and the administration of PARP inhibitor.** C57BL/6 male mice were purchased from Charles River Laboratories Magyarorszag Kft (Isaszeg, Hungary) and kept under standardized, specific pathogen free circumstances. Starting at 8 weeks of age, mice received a diet of powdered rodent chow containing 0.2 % cuprizone (bis-cyclohexanone oxaldihydrazone) (Sigma, Steinheim, Germany) by weight for three, five and six weeks *ad libitum* to induce demyelination, as described previously [Hiremath et al.,1998]. To investigate cuprizone induced changes of the immune system this diet was also given to 4-week-old male mice for one week. The PARP inhibitor 4-hydroxyquinazoline (4HQ, Sigma-Aldrich, Steinheim, Germany) [Banasik et al.,1992] was administered intraperitoneally in a dose of 100 mg/kg body mass and a volume of 10µl/g body mass every day [Veres et al.,2004] started on the same day as the cuprizone-treatment. Control mice received the same volume (10µl/g) of saline solution instead of 4HQ (**Fig. 5**).

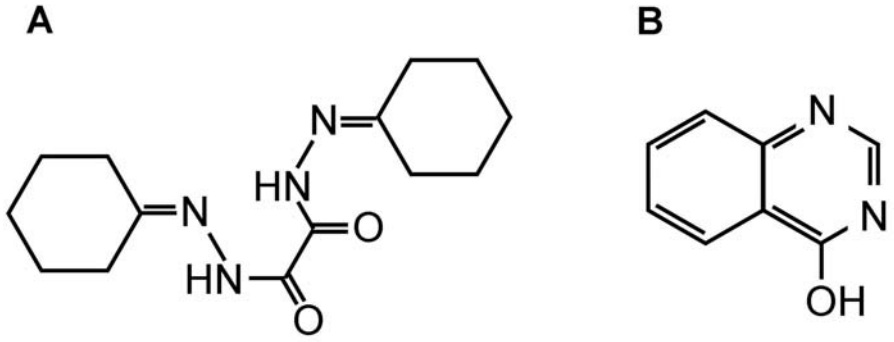


**Fig. 5 Structure of (a) cuprizone (bis-cyclohexanone oxaldihydrazone) and of (b) the PARP inhibitor, 4-hydroxyquinazoline (b).**

All animal experiments were carried out under legislation (1998/XXVIII Act of the Hungarian Parliament on Animal Protection and Consideration and Decree of Scientific Procedures of Animal Experiments (243/1998)) in laboratories of University of Pecs. Licensing of procedures was controlled by The Committee on Animal Research of University of Pecs according to the Ethical Codex of Animal Experiments.

**Measuring body and thymus mass, thymocyte preparation.** In order to follow the systemic effect of cuprizone, mouse weights were recorded at the beginning and after every week of the treatment [Hiremath et al.,1998].

Mice undergoing investigation of the immune system were sacrificed after one week of treatment by rapid decapitation. The chests of mice were cut open, thymi were photographed, dissected carefully and their wet weight was measured. To better determine thymus mass changes upon the treatment a ratio of thymus mass to the whole body mass was calculated. Thymi were then homogenised in PBS (phosphate buffered saline) with a glass/glass homogeniser. The suspension was filtered through nylon mesh and thymocytes were washed once and resuspended in PBS. Separate aliquots of cells were diluted 1:100 and total numbers of cells were counted by Trypan blue method using a hemocytometer and then the cell number of samples was set to $10^6$ except for AnnexinV staining, where $5x10^5$ cells were used.

**Apoptosis detection of thymocytes.** For apoptosis detection, double staining with AnnexinV-FITC (BD Pharmingen, CA) and propidium iodode (PI) (Sigma-Aldrich) was performed according to the method of Vermes et al. (1995). Briefly, $5x10^5$ thymocytes were resuspended in 100 µl Annexin binding buffer (10mM HEPES/NaOH, pH 7.4, 140mM NaCl and 2.5mM $CaCl_2$) and incubated for 20 minutes at room temperature with AnnexinV-FITC in the dark then diluted with 400 µl AnnexinV binding puffer. PI was given to the cells immediately before flow cytometric analysis. Two-parameter dot-plots showing AnnexinV/PI staining (FL1/FL3 channels) were created to determine the ratio of apoptotic cells in the thymic glands.

**Thymocyte fluorescent labelling, flow cytometric acquisition and analysis.** For the simultaneous detection of cell surface CD4, CD8 and CD3 triple labelling technique was used. Thymocyte samples were incubated with monoclonal antibody cocktails for 30 min in 100 ml binding buffer on ice (PBS containing 0.1% $NaN_3$ and 0.1% bovine serum albumin, BSA), then washed twice in PBS and finally resuspended in 500 ml 0.1% buffered paraformaldehyde (PFA) in PBS. Following monoclonal antibodies were used: phycoerythrin (PE) conjugated rat anti-mouse CD4, CyChrome (CyC) conjugated rat anti-mouse CD8 and fluorescein isothyocyanate (FITC) conjugated rat anti-mouse CD3, all purchased from BD Pharmingen, CA. Samples were measured and analysed in a FACSCalibur flow cytometer (Becton Dickinson, San Jose, CA), using the CellQuest software. Generally 10.000 events were recorded. Thymocytes were gated according to their size and granularity on forward and side scatter dot plots. The gate set on untreated

control living thymocytes was used for the analysis of all samples. We used fluorescent dot plots for both comparing the different samples and for calculating the ratio of positively stained cells.

**Immunofluorescence microscopy of thymi.** Frozen thymic sections (7-10 μm thick) were prepared from removed thymi, then fixed in cold acetone, dried and blocked using 5% BSA in PBS for 20 min before staining with anti-Ly51-PE (clone 6C3, BD Biosciences) and anti-EpCAM1-FITC (clone G8.8, hybridome from the Dept. Immunology and Biotechnology, University of Pecs) antibodies to visualize the thymic epithelial network. The remaining sections were stained with anti-CD4-FITC (YTS191.1, hybridome from the Dept. Immunology and Biotechnology, University of Pecs) and anti-CD8-Alexa fluor 647 (clone 53-6.7, BD Biosciences) to investigate the staining pattern of thymocytes. The sections were analysed using an Olympus BX61 microscope equipped with CCD-camera and AnalySIS software.

**Magnetic resonance imaging (MRI) and quantitative neuroimaging.** At the beginning of the treatment and from the third week, mice were anaesthetized weekly by intraperitoneal injection of diazepam (5 mg/kg) and ketamine (80 mg/kg) (both purchased from Gedeon Richter Plc, Budapest, Hungary). The animals were then secured in an epoxy resin animal holder tube (Doty Scientific Inc., Columbia, SC, USA) custom modified to accommodate the tip of teeth and position the eyes of each animal to the same location: 5.0±0.5 mm above the isocenter of the magnet. A glass capillary filled with water:glycerol=9:1 mixture was placed near the head of the animal serving as an external signal intensity reference. MR images were obtained using a Varian INOVA 400 WB NMR spectrometer (Varian Inc., Palo Alto, CA, USA) with an 89-mm vertical bore magnet of 9.4 T (Oxford Instruments Ltd., UK) using a 35-mm inner diameter hollow microimaging probe with a Litz-type transmit/receive volume radio frequency coil and built-in self-shielded water-cooled gradient system with 600 mT/m gradient strength and <100 μs rise time (Doty Scientific Inc., Columbia, SC, USA).

After tuning, manual shimming and radio frequency calibration, coronal cross-sectional images were recorded in a $T_2$-weighted multislice spin echo experiment (TR=3500 ms, TE=40 ms, FOV=25×25 mm) obtaining 21 contiguous slices, each 1.0

mm thick. The acquisition matrix was 128×128, one single average was detected resulting in a total acquisition time of 7.5 min. Images were reconstructed as 256×256 matrices. Postprocessing was performed by VNMR 6.1C and Image Browser (Varian Inc., Palo Alto, CA, USA) softwares on a Sun Ultra 30 workstation (Sun Microsystems, Mountain View, CA, USA).

The extent of demyelination in the corpus callosum was determined calculating mean signal intensity of the corpus callosum divided by mean signal intensity of the reference capillary. Mean signal intensities were determined by freehand delineation of the regions of interest in the corpus callosum or the reference capillary on coronal cross-sectional images exactly 1 mm posterior from the bregma by an investigator blind to the experiment. The extent of hydrocephalus was quantified calculating ventricle volume divided by brain volume. The area of the ventricles was obtained for each slice by freehand delineation of the ventricles and the total volume was estimated from the sum of the areas multiplied by the slice thickness (1.0 mm). The same method was used for estimating brain volume [Harris et al.,1992].

**Histopathology.** After five weeks of treatment mice were terminally anaesthetized with intraperitoneally administered diazepam and ketamine and perfused via the left ventricle with 4% PFA in phosphate buffer containing picric acid. After overnight postfixation in the same fixative, brains were dissected. Brains were embedded in paraffin before histological analysis, then eight μm coronal sections were obtained at the levels of 161, 181, 209 and 221 [Sidman,1971]. Demyelination was evaluated using Luxol fast blue staining with Cresyl violet.

**Immunohistochemistry, immunofluorescence and confocal laser microscopy of cuprizone lesions.** Immunohistochemistry was performed on eight μm thick paraffin sections. Slides were rehydrated, heat-unmasked, blocked in a solution containing 2 % normal horse serum and PBS and incubated overnight with the primary antibody diluted in blocking solution. Primary monoclonal antibody against PAR (1:100, Alexis Biotechnology) was used. Appropriate biotinylated secondary antibody (1:200, Molecular Probes) and 3,3'-diaminobenzidine-tetra-hydrochloride (DAB) reaction was applied for visualization, cell nuclei were counterstained with hematoxylin.

Fluorescent immunohistochemistry was performed on paraffin sections. Staining with primary antibody PAR or AIF (both 1:100, Alexis Biotechnology or Cell Signaling

Technology, respectively) was done overnight. As a second step, sections were incubated with appropriate Alexa Fluor 488-conjugated secondary antibody (1:200, Molecular Probes) or with appropriate biotinylated secondary antibody (1:200, Amersham Pharmacia Biotech), where this first staining was finished by application of streptavidin-Cy2 (Jackson ImmunoResearch, West Grove, PA; 1:75) for one hour at room temperature. After washing in Tris buffered saline (TBS), the sections were incubated overnight with anti-carbonic anhydrase II (The Binding Site Ltd, Birmingham, UK, for detection of oligodendrocytes). This was followed by washing and incubation with appropriate secondary Cy3-conjugated antibody (1:100, Jackson ImmunoResearch). The staining was finished by 4',6'-diamidino-2-phenylindole (DAPI) (Sigma) or by PI (Sigma) counterstain.

Sections were examined using a confocal laser scanning microscope (Leica SP5, Mannheim, Germany, or Olympus FluoView FV-1000). Recordings for Cy2 (excited with the 488-nm laser) and Cy3 (excited with the 543-nm laser) were done simultaneously and was followed by recording for DAPI with a 405 nm laser detected in the blue channel; PI was excited with the 565 nm laser detected in the red channel and Alexa Fluor 488 with the 488 nm laser detected in the green channel, respectively.

**Immunoblot analysis.** Tissue samples were taken from animals sacrificed after three or five weeks of treatment. Corpus callosum of the mice were carefully dissected and 25 mg tissues were homogenized in ice-cold 10 mM Tris buffer, pH 7.4 (containing 0.5 mM sodium metavanadate, 1mM EDTA and protease inhibitor cocktail (1:200); all purchased from Sigma-Aldrich, Steinheim, Germany). Homogenates (10 µg each) were loaded 10% and 12% sodium dodecyl sulphate polyacrylamide gels, electrophoresed and transferred to nitrocellulose membranes. The membranes were blocked in 5% low fat milk for 1.5 h at room temperature then exposed to primary antibodies at 4 ˚C overnight in blocking solution. The following antibodies were used: anti-MBP (1:1000) (Novocastra Laboratories Ltd., Newcastle upon Tyne, U.K.), anti-PAR (1:1000) (Alexis Biotechnology, London, U.K.), anti-AIF (1:330) (Santa Cruz Biotechnology, Santa Cruz, CA, USA), anti-phospho-Akt ($Ser^{473}$) (1:1000) (R&D Systems, Minneapolis, MN, USA), anti-nonphosphorylated Akt/PKB (1:1000), anti-extracellular signal-regulated kinase 1/2 (ERK1/2) ($Thr^{183}/Tyr^{185}$) (1:1000), anti-phospho JNK ($Thr^{183}/Tyr^{185}$) (1:1000), anti-caspase-3 (1:1000) (all from

Cell Signalling Technology, Beverly, MA, USA), anti-phospho-p38-mitogen-activated protein kinase (p38-MAPK) ($Thr^{180}/Tyr^{182}$) (1:1000) and anti-actin (1:10.000) (both from Sigma-Aldrich, Steinhein, Germany). Appropriate horseradish peroxidase-conjugated secondary antibodies were used at a 1:5000 dilution (anti-mouse and anti-rabbit IgGs; Sigma-Aldrich, Steinheim, Germany) and visualized by enhanced chemiluminescence (Amersham Biosciences, Piscataway, New Jersey, USA). Films were scanned, and the pixel volumes of the bands were determined using NIH Image J software (Bethesda, Maryland, USA). For membrane stripping and reprobing membranes were washed in stripping buffer (0.1 M glycine, 5 M $MgCl_2$, pH 2.8) for an hour at room temperature. After washing and blocking, membranes were incubated with primary antibodies for non-phosphorylated or loading control proteins.

**Caspase-3 activity assay.** Carefully dissected corpus callosum samples (20 mg) from animals treated for three weeks were homogenized in lysis buffer (50 mM Tris, pH 8) containing protease inhibitor cocktail (Sigma-Aldrich, Steinheim, Germany). Fluorometric assays were performed using fluorescent-labelled peptide substrate for caspase-3 (Ac-DEVD-AFC, Sigma-Aldrich, St. Louis, MO, USA) and a fluorescence plate reader set at 360 nm excitation and 460 nm emission as recommended by the manufacturer.

**Statistics.** Random effect analysis of variance was performed for comparing the mass and cell count changes of thymi between the different treatment groups. By the evaluation of flow cytometric measurements Student's t-test was used.
The repeated body weight measurements and the time series of relative ventricle volumes were analysed using a random intercept fixed slope linear model considering a common distribution of initial weights or volumes but separate slopes for the treatment groups. Relative corpus callosum MRI signal intensities in the treatment groups were compared with a mixed effect analysis of variance where individuals were modelled as random effects. The immunoblot band intensities in the four treatment groups were normalized to the loading control and compared pairwise using Scheffé's post hoc ANOVA test, heteroscedasticity was minimised with logarithmic transformation. Differences were considered significant at values of $p<0.05$ or lower.

## 4. RESULTS

### 4.1 Effects of PARP inhibition on weight loss, hydrocephalus formation and demyelination induced by cuprizone

#### 4.1.1 PARP inhibitor attenuated cuprizone-induced weight loss

During the six weeks of the treatment 8-week-old control mice showed increasing body masses (0.48 g/week, $p<0.001$). Similar weight gain was observed in the 4HQ treated group (0.38 g/week, $p<0.001$), while cuprizone treated animals showed severe weight loss throughout the six weeks (-1.35 g/week, $p<0.001$, **Fig. 6**). In the cuprizone and 4HQ treated group we did not find any major change in the body mass of the animals (-0.07 g/week, $p=0.22$, **Fig. 6**).

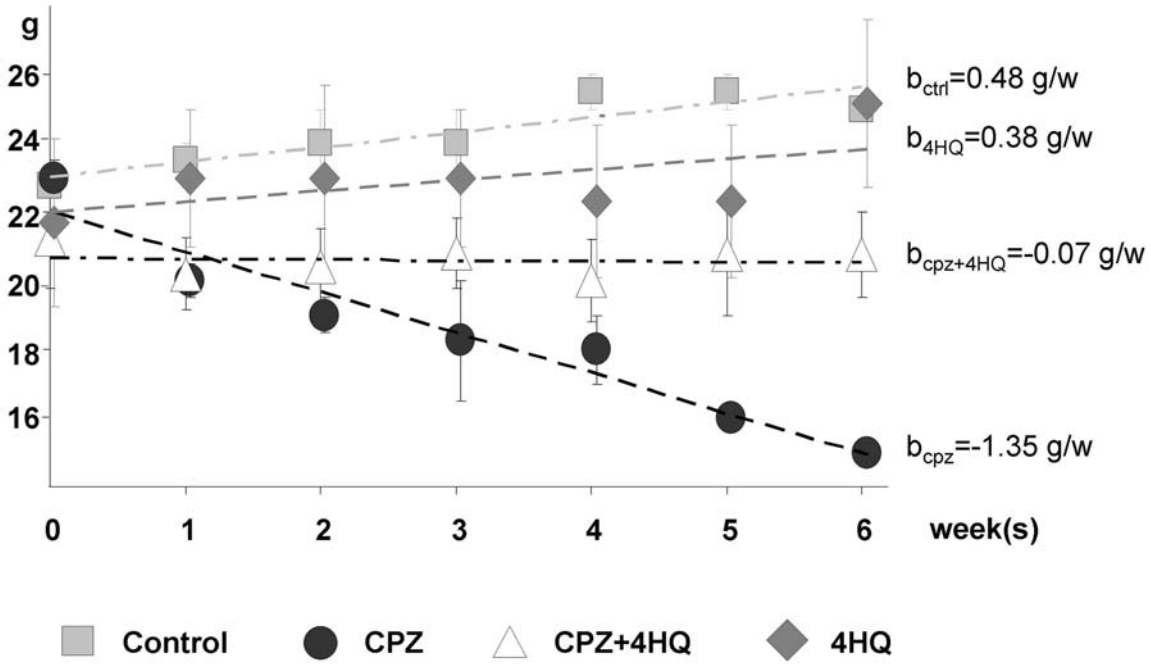


**Fig. 6 Body mass changes of 8-week-old mice upon cuprizone and 4HQ treatment for six weeks.** Results are expressed as mean body mass ±SD of all the 120 mice included in this study. Random intercept fixed slope linear model was used to determine weekly growth rates (b) indicated at the right edge of the figure. (CPZ: cuprizone, 4HQ: 4-hydroxiquinazoline)

Cuprizone treatment thus caused significant weight loss in comparison to the control group (difference: -1.82 g/week, $p<0.001$), which was effectively prevented by the simultaneous administration of PARP inhibitor (difference: 1.28 g/week, $p<0.001$). Growth rate of the cuprizone and 4HQ treated animals was however still lower than in

the control group (difference: -0.55 g/week, p<0.001). 4HQ affected the growth rate to a small extent only when compared to control (difference: -0.10 g/week, p=0.28, **Fig. 6**).

Cuprizone administration to 4-week-old mice for one week resulted in a significant decrease in their body mass compared to control (p<0.05, **Fig. 7**). This weight loss was reversed when mice were co-treated with the PARP inhibitor 4HQ (p<0.05), moreover the administration of the PARP inhibitor alone did not affect their body mass (p=0.66, **Fig. 7**).

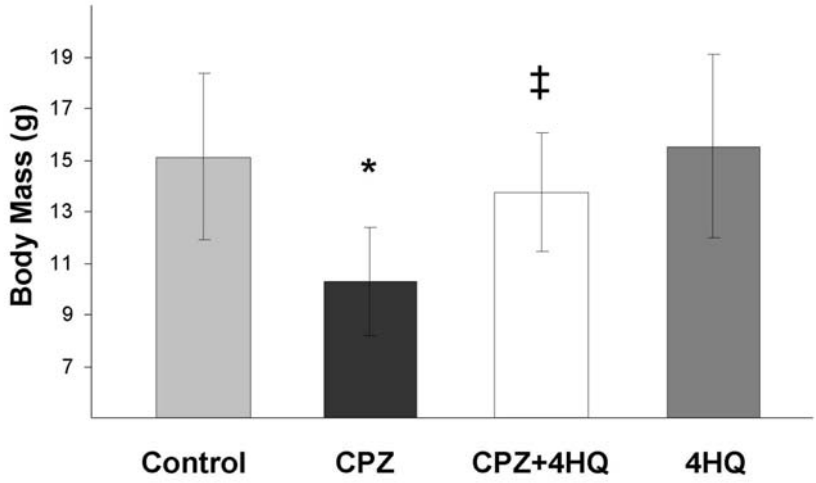


**Fig. 7 Body mass changes of 4-week-old mice upon cuprizone and 4HQ treatment for one week.** Results are expressed as mean body mass (g) ±SD. *p<0.05 compared to control group; ‡p<0.05 compared to cuprizone treated group. Experiments were repeated three times and at least three mice were included in each group in all experiments. (CPZ: cuprizone, 4HQ: 4-hydroxiquinazoline)

### 4.1.2 PARP inhibition prevented cuprizone-induced hydrocephalus formation

Examination of the brain was performed by serial, non-invasive *in vivo* magnetic resonance neuroimaging. Brain ventricles appear due to their liquor cerebrospinalis content extremely hyperintense in $T_2$-weighted images. Administration of cuprizone caused severe hydrocephalus, i.e. dilation of all four brain ventricles, which was the most pronounced by the end of the sixth week (**Fig. 8**). Quantification of relative brain ventricle volume (ventricle volume/ brain volume) revealed significant dilation already by the fourth week of the treatment, which was even more pronounced thereafter (p<0.001, **Fig. 9**). Co-treating mice with 4HQ prevented formation of hydrocephalus during the whole experiment (p<0.001, **Fig. 9**). Administration of the PARP inhibitor alone did not affect the volume of brain ventricles (**Fig. 9**).

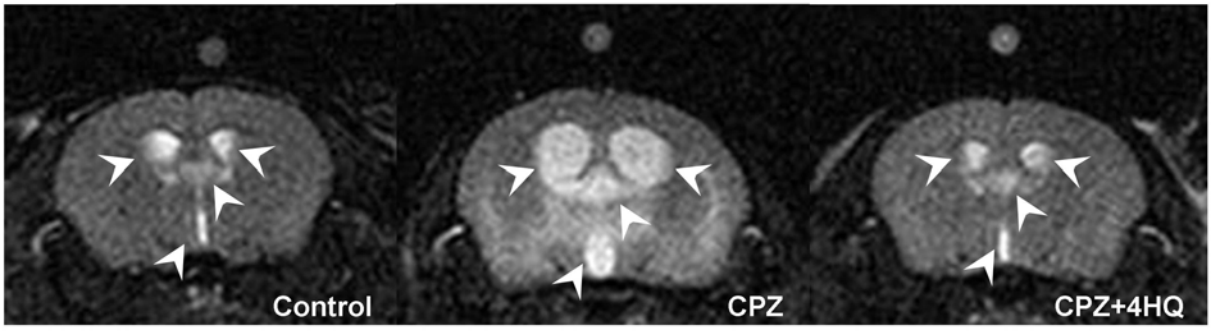


**Fig. 8 Changes of $T_2$-weighted MR images of brain coronal sections upon cuprizone and 4HQ treatment.** Representative $T_2$-weighted spin echo MR images of brain coronal sections of control (left panel), cuprizone-treated (middle panel) and cuprizone and 4HQ-treated mice (right panel) treated for six weeks. Arrowheads indicate brain ventricles filled with hyperintense appearing liquor cerebrospinalis. Experiments were repeated three times and at least five mice were included in each group in all experiments. (CPZ: cuprizone, 4HQ: 4-hydroxiquinazoline)

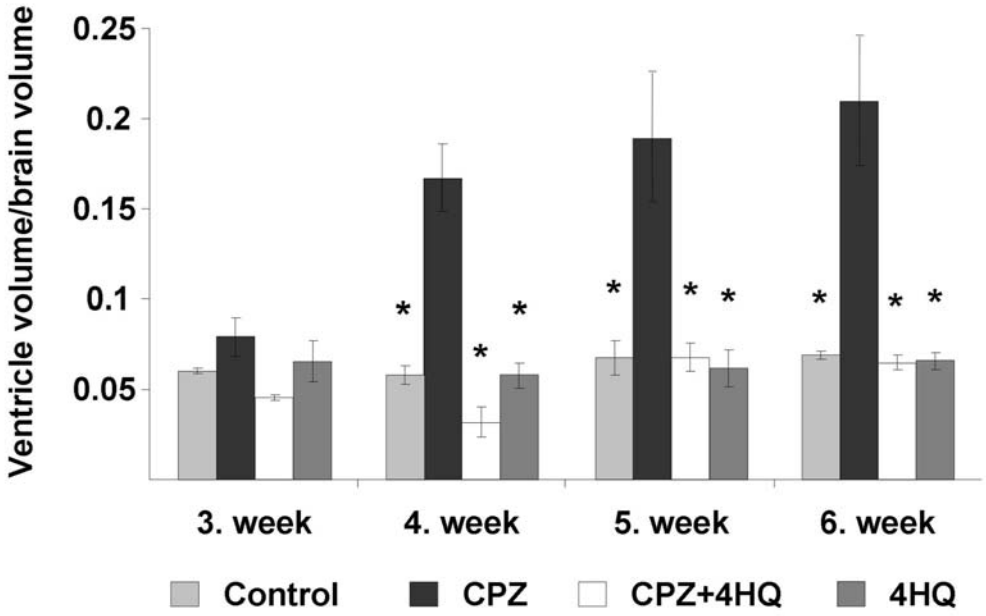


**Fig. 9 Effect of cuprizone and 4HQ treatment on the relative ventricle volume of mice.** Quantification of hydrocephalus in mice treated for six weeks was performed by determining ventricle volume and brain volume ratios. Data are expressed as mean volume ratios ±SD. *p<0.001 compared to control group. Experiments were repeated three times and at least five mice were included in each group. (CPZ: cuprizone, 4HQ: 4-hydroxiquinazoline)

### 4.1.3 PARP inhibition protected from cuprizone induced demyelination in the brain

In $T_2$-weighted magnetic resonance images corpus callosum appeared hypointense in control mice. Upon cuprizone treatment corpus callosum showed hyperintensity suggestive of demyelination, which was reversed by the administration of 4HQ (**Fig. 10**).

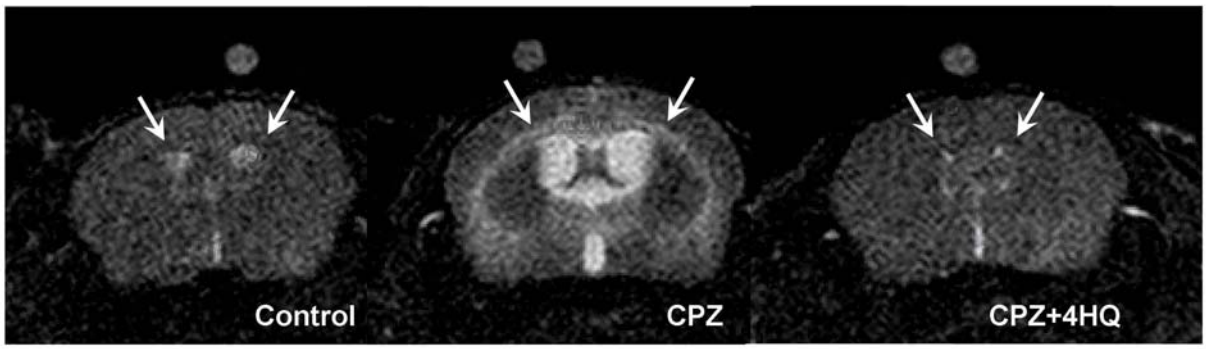


**Fig. 10 Changes of $T_2$-weighted MR images of brain coronal sections upon cuprizone and 4HQ treatment.** Representative $T_2$-weighted spin echo MR images of brain coronal sections of mice treated for four weeks. Arrows indicate hyperintensities (suggesting demyelination) or hypointensity (intact myelin status) in corpus callosum. Experiments were repeated three times and at least five mice were included in each group in all experiments. (CPZ: cuprizone, 4HQ: 4-hydroxiquinazoline)

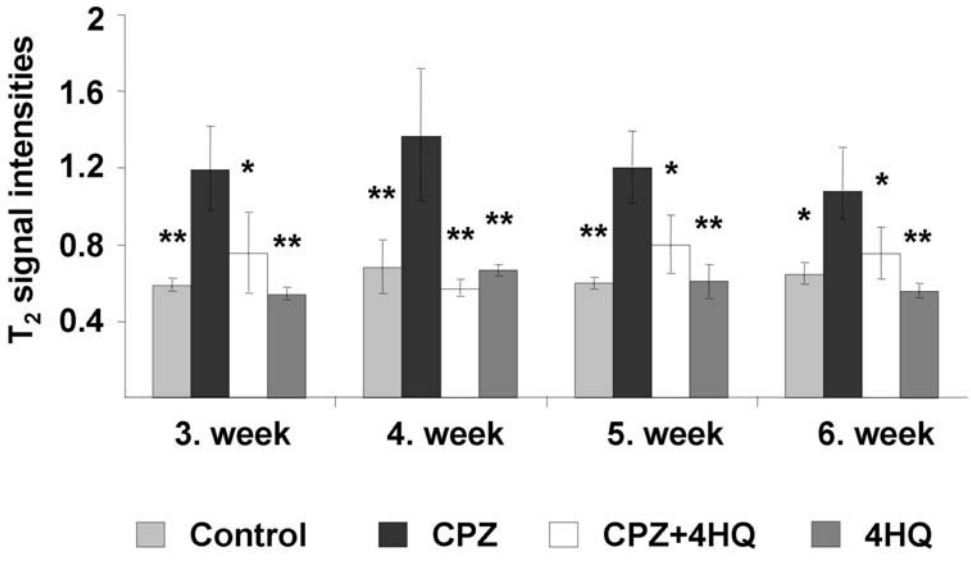


**Fig. 11 Effect of cuprizone and 4HQ treatment on the $T_2$ signal intensities in the corpus callosum.** Quantification of $T_2$ intensity changes in the corpus callosum of mice treated for six weeks. Data are expressed as normalized mean signal intensities ±SD. *p<0.05 compared to cuprizone group, **p<0.01 compared to cuprizone group.

Experiments were repeated three times and at least five mice were included in each group. (CPZ: cuprizone, 4HQ: 4-hydroxiquinazoline)

Quantitative analysis of serial measurements revealed a significant increase of normalized corpus callosum signal intensity already by the third week of cuprizone treatment when compared to control ($p<0.01$, **Fig. 11**). This increase was the most pronounced on the fourth week of the treatment, $T_2$-weighted corpus callosum signal intensity decreased thereafter but remained still significantly higher compared to control ($p<0.01$ or $p<0.05$ respectively, **Fig. 11**). Co-administration of PARP inhibitor resulted in significantly lower signal intensities throughout the experiment ($p<0.01$ or $p<0.05$ respectively, **Fig. 11**). When applied alone, 4HQ did not cause any changes in signal intensities (**Fig. 11**).

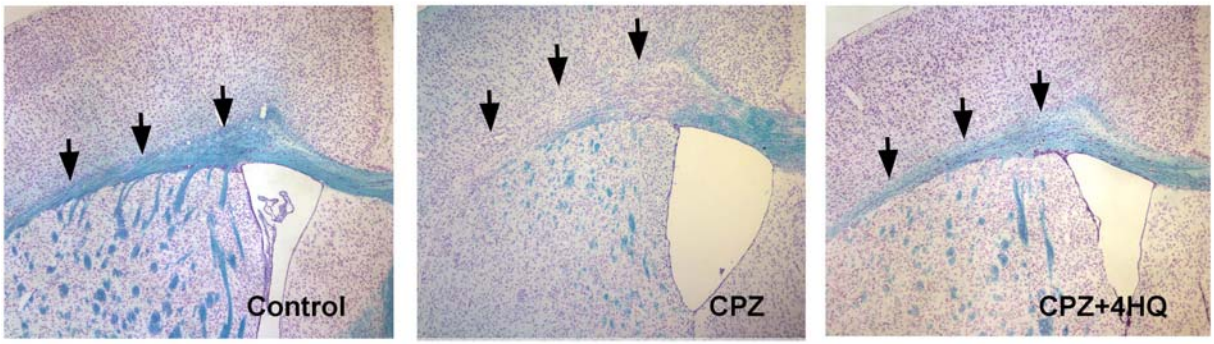


**Fig. 12 Changes of the myelin status of the corpus callosum upon cuprizone and 4HQ treatment.** Representative histopathology images of the corpus callosum (*arrows*) on brain coronal sections of mice treated for five weeks. Blue staining by Luxol fast blue indicates intact myelin sheath. Experiments were repeated at least three times and at least five mice were included in each group. (CPZ: cuprizone, 4HQ: 4-hydroxiquinazoline)

Pathological analysis with luxol fast blue-Cresyl violet staining showed a profound myelin loss in the corpus callosum of mice after five weeks of cuprizone treatment (**Fig. 12**). 4HQ reduced the cuprizone-induced demyelination (**Fig. 12**), meanwhile 4HQ alone did not affect myelination (*data not shown*).

In order to quantify the myelin amount in the corpus callosum upon cuprizone and 4HQ treatment, a quantitative myelin basic protein (MBP) immunoblotting was performed. MBP immunoblotting revealed significantly decreased MBP expression after five weeks of cuprizone feeding compared to control ($p<0.01$), which was significantly reversed by the PARP inhibitor 4HQ ($p<0.05$). Administration of the PARP inhibitor alone did not affect the MBP level (**Fig. 13**).

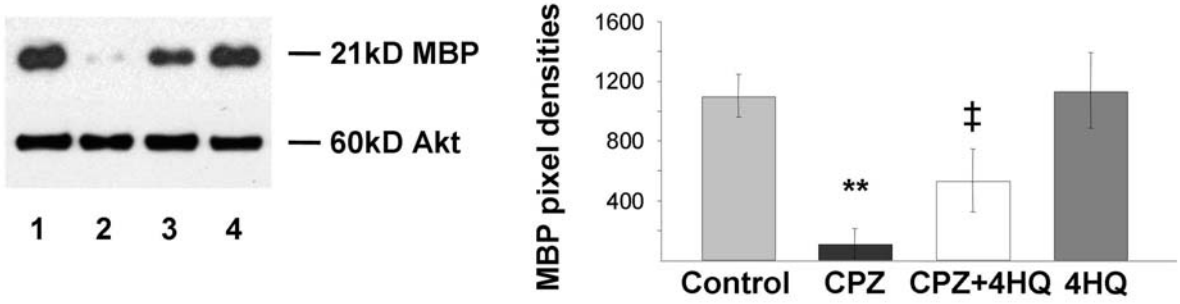


**Fig. 13 Effect of cuprizone and 4HQ treatment on the MBP expression in the corpus callosum.** MBP expression in the dissected corpus callosum of mice treated for five weeks was detected by immunoblotting utilizing an anti-MBP antibody. Even protein loadings were confirmed by an anti-Akt antibody and immunoblotting. Representative immunoblots (left panel) from three experiments with similar results and densitometric evaluation (right panel) are shown. At least five mice were included in each group.
*Lane 1*, control; *lane 2*, cuprizone (CPZ) treatment*; lane 3*, cuprizone+4HQ (CPZ+4HQ) treatment; *lane 4*, 4HQ only. Results on diagram are expressed as mean pixel densities ±SD; **p<0.01 compared to control; ‡p<0.05 compared to cuprizone group. (CPZ: cuprizone, 4HQ: 4-hydroxiquinazoline)

## 4.2 Effects of cuprizone and PARP inhibition on thymi of mice

### 4.2.1 Cuprizone treatment induced acute thymic atrophy

In order to investigate the effect of cuprizone on thymi, 4-week-old male C57BL/6 mice were treated with cuprizone. Already after one week of cuprizone administration severe thymic atrophy could be observed (**Fig. 14**) that was accompanied by significant thymic tissue mass loss when compared to control ($p<0.05$) (**Fig. 15a**).

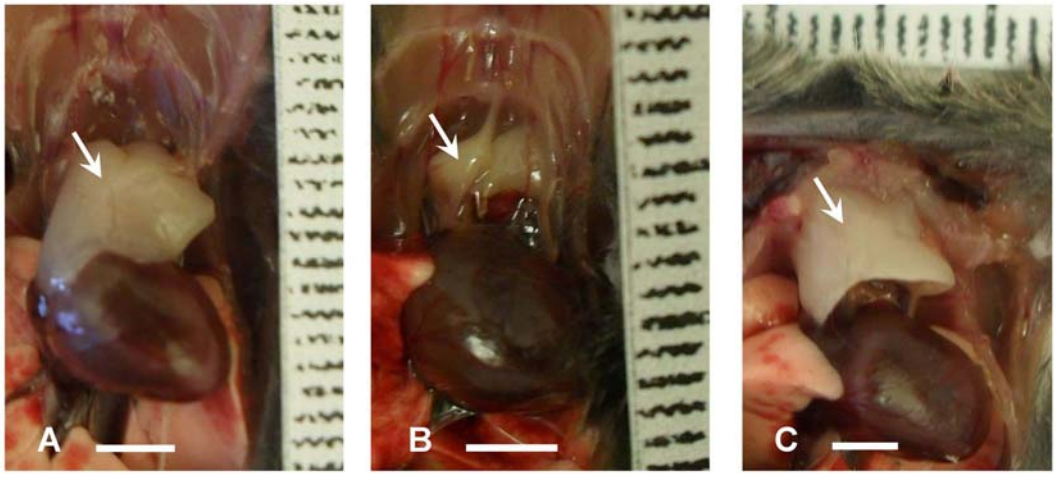


**Fig. 14 Macroscopic changes of thymi upon cuprizone and 4HQ treatment.** 4-week-old male mice were treated with cuprizone and 4HQ for one week. Representative photograph of the open chest of a control (**a**), cuprizone treated, (**b**) and a cuprizone and 4HQ treated animal (**c**). Arrows indicate thymi of mice. Scale bars indicate 3 mm. Experiments were repeated three times and at least three mice were included in each group in all experiments.

Since cuprizone treatment resulted in a significant weight loss of the animals (**Fig 7**), we considered the possibility that the decrease of thymus tissue mass was due to general adipose tissue loss. Therefore we normalized the thymus tissue mass to the whole body mass and determined absolute thymocyte number. The thymus tissue mass/ whole body mass ratio (relative thymus mass) was still significantly lower after one week of cuprizone treatment compared to control ($p<0.01$) (**Fig. 15b**). Absolute thymocyte number was also found to be significantly lower upon cuprizone treatment compared to control ($p<0.001$) (**Fig. 15c,d**).

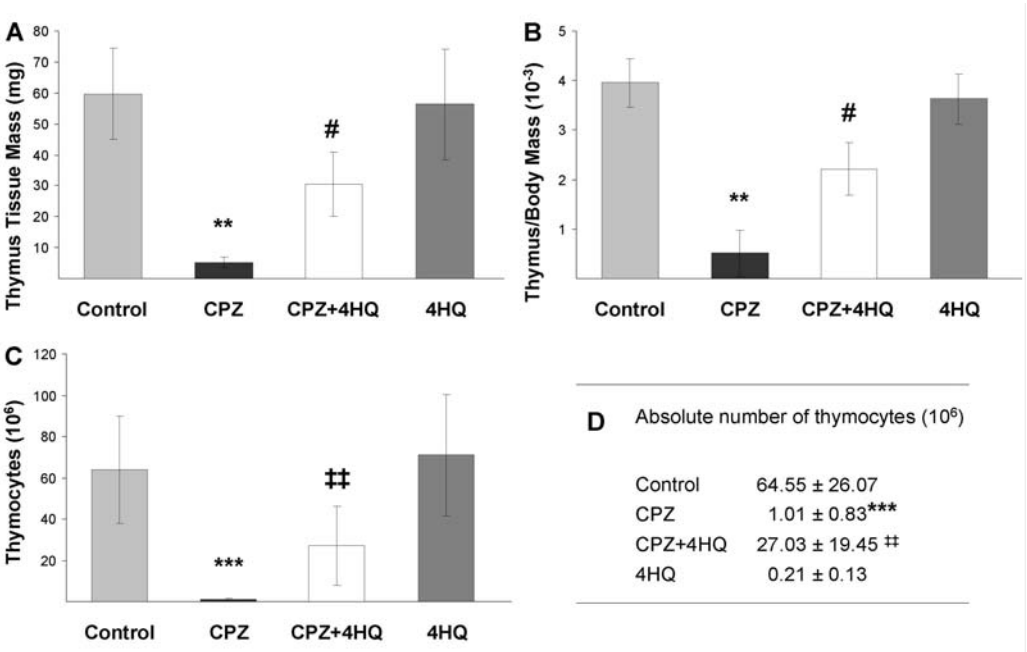


**Fig. 15 Effect of cuprizone and 4HQ treatment on thymus mass and thymocyte number of mice.** 4-week-old male mice were treated with cuprizone and 4HQ for one week. (**a**) Mean thymus mass (mg), (**b**) mean relative thymus mass (thymus tissue mass/ whole body mass) ($x10^{-3}$), (**c, d**) mean absolute number of thymocytes ($x10^{6}$). ±SD; **p<0.01 compared to control group; ***p<0.01 compared to control group; #p<0.01 compared to cuprizone group, ‡‡p<0.001 compared to cuprizone group. Experiments were repeated three times and at least three mice were included in each group in all experiments. (CPZ: cuprizone, 4HQ: 4-hydroxiquinazoline)

### 4.2.2 Cuprizone induced apoptotic cell death of thymocytes exerting the strongest effect on $CD4^+$, $CD8^+$ double positive T cells

To investigate, whether the observed severe thymic atrophy was due to massive thymocyte death, we performed FITC-conjugated AnnexinV/ propidium iodide (PI) double staining on thymocytes of cuprizone-treated mice. PI intercalates into double-stranded nucleic acids and is excluded by viable cells but can penetrate cell membranes of dying or dead cells. As AnnexinV detects phosphatydilserine exposure in the cell membrane of apoptotic cells, the AnnexinV/PI staining technique can differentiate between normal (double negative), early apoptotic (AnnexinV single positive), and late apoptotic or necrotic (AnnexinV and PI double positive) cells.

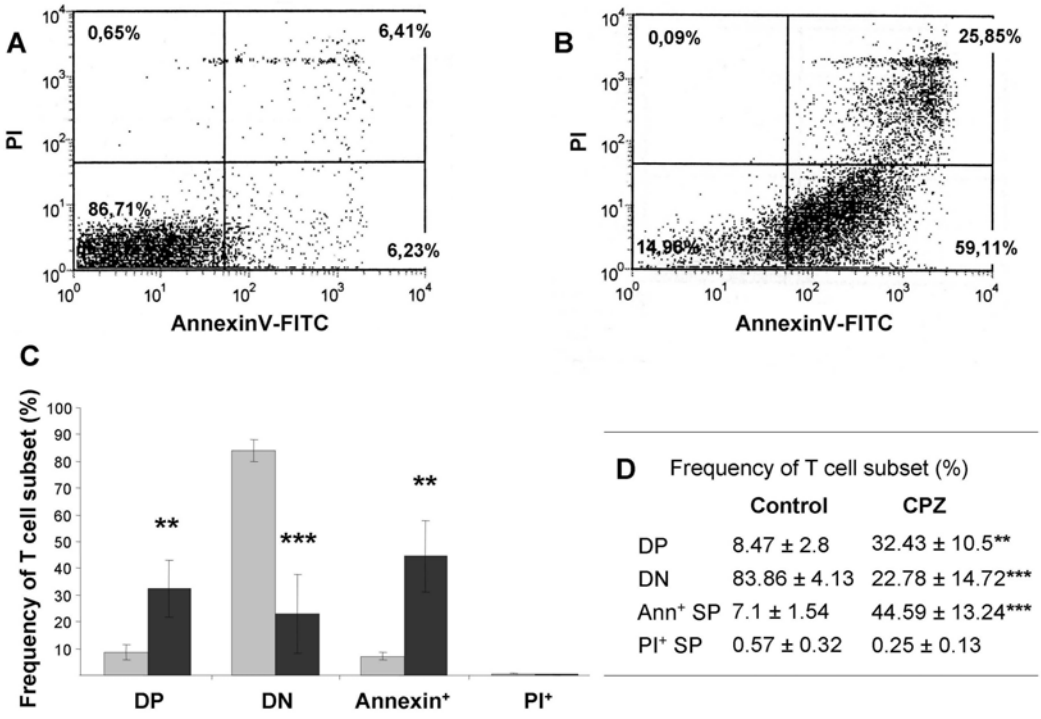


**Fig. 16 AnnexinV/ propidium iodide analysis of T cells after cuprizone treatment.** Representative AnnexinV-PI dot-plot of the thymocytes of a untreated animal (**a**) and an animal treated with cuprizone for one week (**b**). Numbers indicate percent ratio of double negative (normal, lower left quadrant), AnnexinV single positive (early apoptotic, lower right quadrant) and double positive (late apoptotic/necrotic, upper right quadrant) populations. (**c,d**) Frequency of thymocyte subsets in control (light grey) and cuprizone treated (dark grey) mice. DP: double positive, DN: double negative, $Ann^+$ SP: AnnexinV single positive, $PI^+$ SP: propidium iodide single positive; *p<0.05 compared to control, **p<0.01 compared to control, ***p<0.001 compared to control. Experiments were repeated three times and at least three mice were included in each group in all experiments. (CPZ: cuprizone)

Flow cytometric analysis of the whole thymocyte population showed that most of the thymocytes of untreated control mice bound neither AnnexinV nor PI (83.86 ± 4.13%, **Fig. 16a,d**), suggestive of a normal thymocyte population. Analysis of thymocytes from cuprizone treated animals revealed significant decrease in the percent ratios of the normal cells (22.78 ± 13.24%, p<0.001, **Fig. 16b,d**) accompanied by significantly higher percent ratios of the early apoptotic and late apoptotic (or necrotic) cells compared to control (44.59 ± 13.24%, p<0.001 and 32.43 ±10.5%, p<0.01, respectively **Fig. 16**). Altogether, these data indicated that upon cuprizone treatment thymocytes were dying by apoptosis.

To further investigate the observed thymocyte loss anti-CD4 and anti-CD8 immunofluorescence microscopy was carried out. In merged images of thymi from

control animals the cortex appeared yellow as it is mainly occupied by $CD4^+$ $CD8^+$ DP thymocytes and the medulla occurred rather green because of the predominance of $CD4^+$ SP cells (**Fig. 17**). Cuprizone treatment resulted in severe thymocyte depletion causing almost the disappearance of the double staining areas, a relative growth of the $CD4^+$ areas and a generally weak staining of the shrunk thymus (**Fig. 17**). This serious picture of thymic atrophy was in accordance with the great decrease of thymocyte numbers.

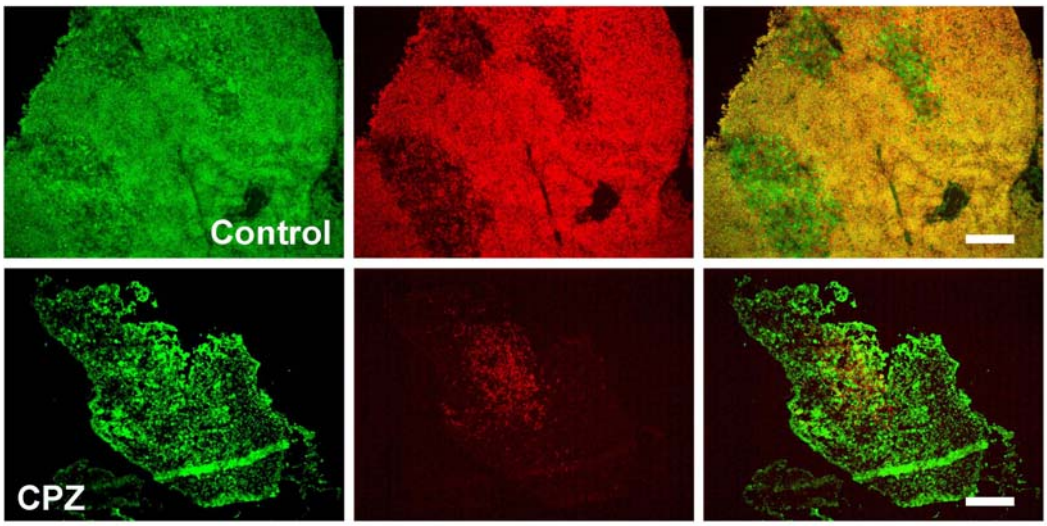


**Fig. 17 Effect of cuprizone treatment on the CD4/CD8 staining pattern of thymi.**
Immunostaining with FITC-labelled anti-CD4 (green) and Alexa647-labelled anti-CD8 (red) antibodies was performed on thymic sections after one week of cuprizone treatment.
Representative images of the green channel (left panels), the red channel (middle panels) and merged images (right panels) of control (upper line) and cuprizone treated (lower line) mice were gained by fluorescent microscopy. Photographs were taken using a 10x objective, scale bar indicates 200 µm. (CPZ: cuprizone)

In order to characterize the remaining living thymocyte population, labelling of thymocytes with fluorescent conjugated anti-CD4 and anti-CD8 antibodies and flow cytometric analysis was performed. To exclude dead or apoptotic cells, the gate was set on untreated control living thymocytes and used for the analysis of all samples.

In case of the 5-week-old male C57BL/6 control mice we found that the most considerable population was the $CD4^+CD8^+$ DP thymocytes that comprised 73.37 ± 2.6% of the whole population (**Fig. 18a**). The most immature $CD4^-CD8^-$ DN thymocytes gave 9.81 ± 5.26%, $CD4^+$ or $CD8^+$ SP thymocytes represented about 15% of the total population, with an approximately double contribution of the $CD4^+$ SP

thymocytes (11.56 ± 2.16% for $CD4^+$ and 5.25 ± 1.67 % for $CD8^+$ SP cells **Fig. 18c,d**).

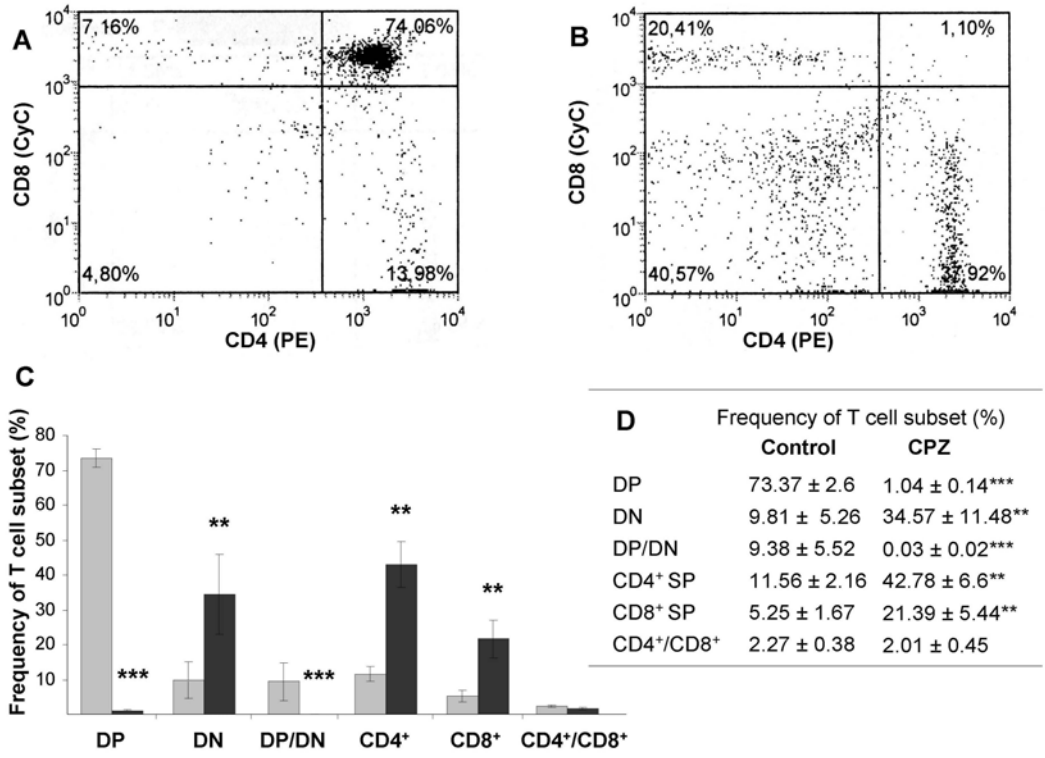


**Fig. 18 Changes of thymocyte subpopulations upon cuprizone treatment.** Representative CD4/CD8-defined cytofluorometric dot-plot profile of normal thymocytes (**a**) and after one week of cuprizone treatment (**b**). Numbers indicate percent ratio of $CD4^+/CD8^+$ double positive (DP, upper right quadrant), $CD4^-/CD8^-$ double negative (DN, lower left quadrant), $CD4^+$ single positive ($CD4^+$, lower right quadrant) and $CD8^+$ single positive ($CD8^+$, upper left quadrant) T cell populations. (**c,d**) Frequency of thymocyte subsets in control mice (light grey) and after one week of cuprizone treatment (dark grey). DP: double positive, DN: double negative, $CD8^+$ SP: $CD8^+$ single positive, $CD4^+$ SP: $CD4^+$ single positive; *p<0.05 compared to control, **p<0.01 compared to control, ***p<0.001 compared to control. Experiments were repeated three times and at least three mice were included in each group in all experiments. (CPZ: cuprizone)

One week of cuprizone treatment resulted in significantly lower percent ratios of the $CD4^+CD8^+$ DP thymocytes (1.04 ± 0.14%, p<0.001, **Fig. 18b,d**). If we take also into consideration the decrease in the total thymocyte number from $65x10^6$ control level to to $1x10^6$ upon cuprizone treatment, this suggests the almost total disappearance of the DP population, indicate also by anti-CD4, anti-CD8 immunohistochemistry. Concomitant with this phenomenon, a significant increase was detected in the percent ratios of the $CD4^-CD8^-$ DN as well as that of the $CD4^+$ and the $CD8^+$ SP populations when compared to control (34.57 ± 11.48%, p<0.01;

39.28 ±6.6%, p<0.001; and 25.11 ± 5.44%, p<0.001, respectively, **Fig. 18c,d**). The degree of the increase in the ratios was found to be about the same DN=3.5 (DN control: 9.8%, DN cuprizone: 34.6%); $CD4^+$=3.7 ($CD4^+$ control: 11.56%, $CD4^+$ cuprizone: 42.8%); $CD8^+$=4.08 ($CD8^+$ control: 5.25%, $CD8^+$ cuprizone: 21.4%). This led also to a significantly lower DP/ DN thymocyte ratio of the cuprizone treated group when compared to control (p<0.001, **Fig. 18c,d**). Although there was a significant increase in the percent ratios of both $CD4^+$ and $CD8^+$ SP cells, the $CD4^+$/$CD8^+$ ratio remained about the same (**Fig. 18c,d**).

### 4.2.3 Cuprizone induced structural changes of the thymic epithelial network

Since there is a symbiotic relationship between developing thymocytes and TECs alterations to the thymic microenvironment was examined. EpCAM is expressed on the surface of all thymic epithelial cells however medullary epithelial cells (mTEC) express higher levels of EpCAM, than cortical epithelial cells (cTEC). Cortical epithelial cells coexpress the Ly-51 cell-surface differentiation glycoprotein ($EpCAM^+Ly\text{-}51^+$), whereas medullary epithelial cells do not express this marker ($EpCAM^{++}$, $Ly\text{-}51^-$) (**Fig. 19**).

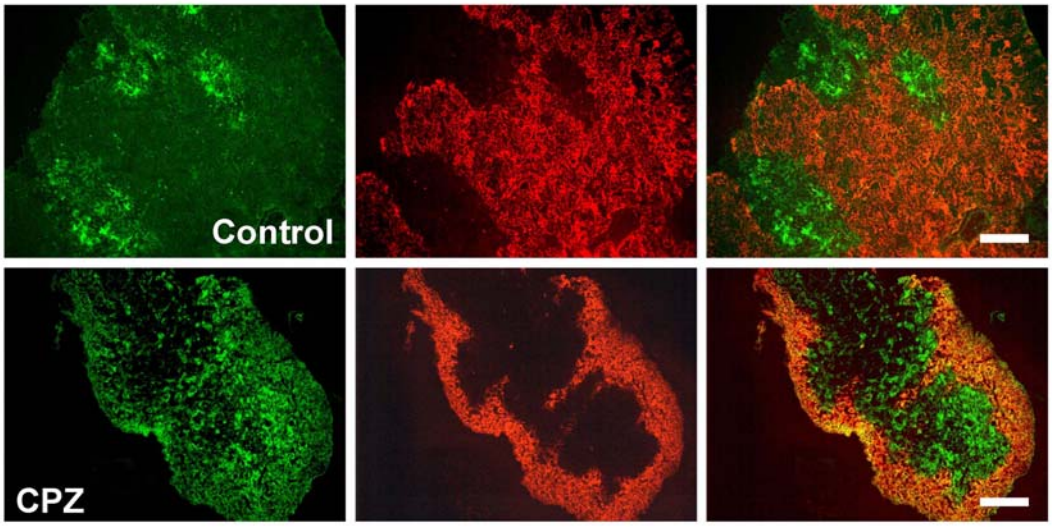


**Fig. 19 Effect of cuprizone on thymic epithelial cells.** Immunostaining with FITC-labelled anti-EpCAM1 (green) and PE-labelled anti-Ly-51 (red) antibodies was performed on thymic sections after one week of cuprizone treatment.
Representative images of the green channel (left panels), the red channel (middle panels) and merged images (right panels) of control (upper line) and cuprizone treated (lower line) mice were gained by fluorescent microscopy. Photographs were taken using a 10x objective, scale bar indicates 200 µm. (CPZ: cuprizone)

Therefore we performed EpCAM/Ly-51 immunofluorescent staining to investigate thymic stromal changes. In merged images of untreated mice mTEC appeared green ($EpCAM^{++}$), whereas cTEC rather orange because of weak green ($EpCAM^{+}$) and strong red ($Ly\text{-}51^{+}$) staining. TECs formed a sponge-like meshwork enabling migration of developing T cells and –although slightly varying between slides– the amount of cTECs (cortex) was always found to be larger than of mTECs (medulla) (**Fig. 19** upper line). Upon cuprizone treatment a general decrease in cellularity, affecting both cTECs and mTECs, was observed with a loss of the sponge-like staining pattern (**Fig. 19** lower line).

### 4.2.4 PARP inhibition attenuated thymic atrophy

Co-administration of the PARP inhibitor 4HQ with cuprizone to 4-week-old male C57BL/6 mice protected them from cuprizone induced severe thymic atrophy (**Fig. 14**). Thymus tissue mass, relative thymus mass and the absolute thymocyte number were found to be also significantly higher after one week of treatment compared to animals treated with cuprizone only ($p<0.01$ respectively, **Fig. 15a-c**). 4HQ treatment alone did not affect the thymus mass, whole body mass or the thymocyte number of mice (**Fig. 15a-c**).

## 4.3 Mechanisms underlying cuprizone induced oligodendrocyte death and its prevention by PARP inhibition

### 4.3.1 Cuprizone enhanced PARP activation in the corpus callosum

In order to investigate the effect of PARP inhibition on experimental demyelination, first we examined whether cuprizone treatment affected the activity of PARP. Since measuring PARP activity *in situ* and *in vivo* was technically difficult, we determined steady state accumulation of the product of the enzyme, poly(ADP-ribose) (PAR), using anti-PAR antibody and immunoblotting, immunohistochemistry or immunofluorescence instead.

Cuprizone induced auto-poly(ADP-ribosyl)ation reflecting to activation of PARP in corpus callosum of mice after three weeks of treatment ($p<0.05$) (**Fig. 20**).

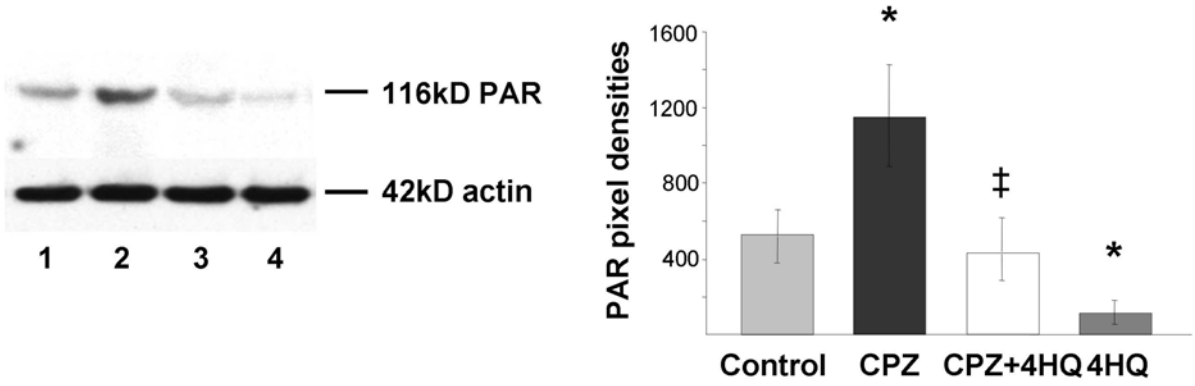


**Fig. 20 Effect of cuprizone and 4HQ treatment on the auto-ADP-ribosylation of PARP in the corpus callosum.** Representative immunoblots for PARP auto-ADP-ribosylation (left panel) and their densitometric evaluation (right panel). Auto-ADP-ribosylation of PARP in the dissected corpus callosum of mice treated for three weeks was detected by immunoblotting utilizing an anti-ADP-ribose antibody. Even protein loadings were confirmed by an anti-actin antibody and immunoblotting. Experiments were repeated three times and at least five mice were included in each group in all experiments.
*Lane 1*, control; *lane 2*, cuprizone treatment (CPZ)*; lane 3*, cuprizone+4HQ (CPZ+4HQ) treatment; *lane 4*, 4HQ only. Results on diagram are expressed as mean pixel densities ±SD; *$p<0.05$ compared to control group; ‡$p<0.05$ compared to cuprizone group.

Anti-PAR immunohistochemistry revealed very strong PAR reactivity in the nucleus and cytoplasm of single cells, predominantly located in the affected areas and containing high numbers of apoptotic cells. The expression was seen in cells which by the anatomy of their processes mainly resembled oligodendrocytes (**Fig. 21** left panel). As demonstrated by immunofluorescence and confocal laser microscopy,

majority of cells that contained condensed, sometimes fragmented nuclei expressed also carbonic anhydrase II (CAII) oligodendrocyte marker (**Fig. 21** insert in left panel). Double staining and confocal laser microscopy also confirmed that the majority of cells with strong PAR immunoreactivity also expressed the oligodendrocyte marker CAII (**Fig. 21,** right panels). Altogether, these data indicated activation of PARP in the nucleus of oligodendrocytes in cuprizone-induced lesions.

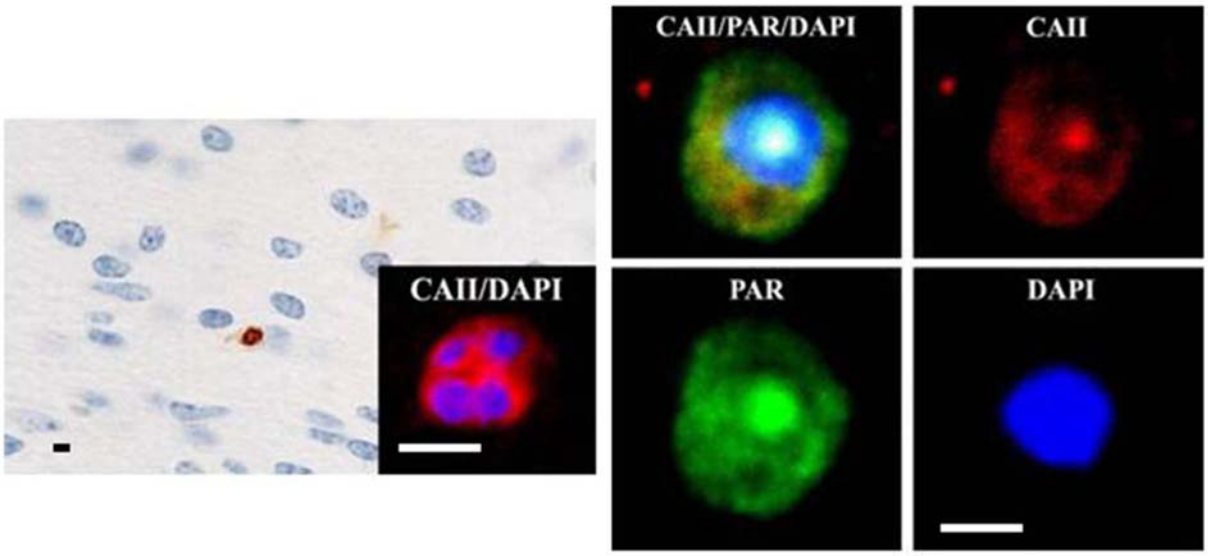


**Fig. 21 Effect of cuprizone treatment on the nuclear activation of PARP in oligodendrocytes.** Representative anti-PAR immunohistochemistry image of corpus callosum in a mouse treated with cuprizone for three weeks (left panel). Brown colour indicates strong PAR reactivity in the nucleus of an oligodendrocyte with condensed nuclei in a cuprizone-induced lesion (arrow). The insert indicates an apoptotic oligodendrocyte stained for carboanhydrase II (CAII) as a marker for oligodendrocytes and DAPI, showing the fragmented nucleus (scale bar: 10 μm). Representative confocal images of PARP activation in an oligodendrocyte (right panels). CAII immunoreactivity (red), PAR immunoreactivity (green) and DAPI nuclear staining (blue) were presented individually and merged (scale bar: 10 μm).

In addition, 4-hydroxyquinazoline (4HQ), a potent inhibitor of the PARP enzyme [Banasik et al.,1992] blocked both cuprizone induced and basal auto-poly(ADP-ribosyl)ation at a dose of 100 mg/kg used throughout this study ($p<0.05$, respectively) (**Fig. 20**). This dose of 4HQ was previously found to be effective and devoid of any apparent toxic effect [Veres et al.,2004].

### 4.3.2 Cuprizone induced caspase-independent AIF mediated cell death in the corpus callosum, which was diminished by PARP-inhibitor

Parallel to demyelination and PARP activation, we observed significantly elevated level of AIF in the corpus callosum of mice treated with cuprizone for three weeks compared to control ($p<0.05$, **Fig. 22**). Administration of the PARP inhibitor 4HQ attenuated this effect significantly ($p<0.05$, **Fig. 22**), although did not alter the expression level of AIF when applied alone (**Fig. 22**).

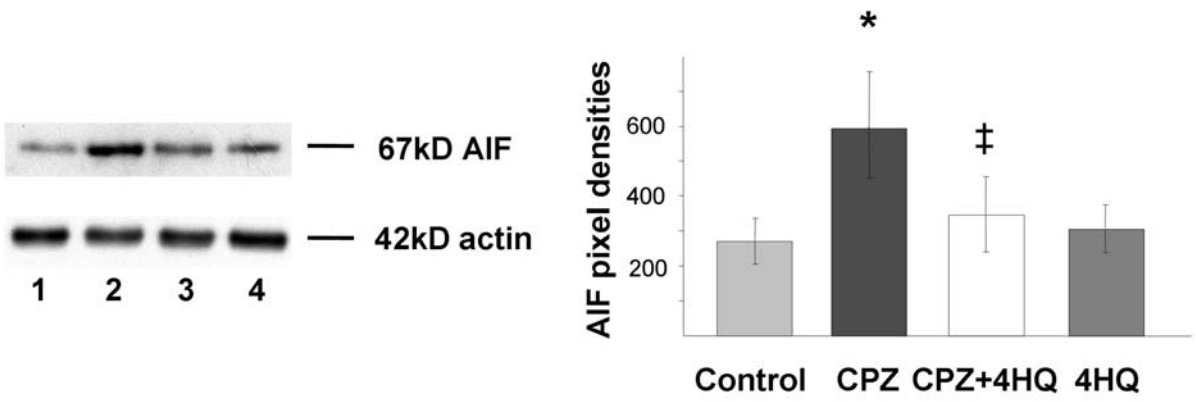


**Fig. 22 Changes of the AIF expression in the corpus callosum upon cuprizone and 4HQ treatment.** Representative immunoblots from three experiments (at least five mice in each group) (left panel) and their densitometric evaluations are shown (right panel). AIF expression in the dissected corpus callosum of mice treated for three weeks was detected by immunoblotting utilizing an anti-AIF antibody. Even protein loadings were confirmed by anti-actin antibody and immunoblotting.
*Lane 1*, control; *lane 2*, cuprizone (CPZ) treatment*; lane 3*, cuprizone and 4HQ (CPZ+4HQ) treatment; *lane 4*, 4HQ treatment. Results on diagram are expressed as mean pixel densities ±SD; *$p<0.05$ compared to control; ‡$p<0.05$ compared to cuprizone group.

Besides elevating its expression, cuprizone induced nuclear translocation of AIF. In cuprizone treated mice, numerous cells showing typical shape and arrangement of oligodendrocytes gave strong nuclear anti-AIF immunostaining in the midline and cingular part of the corpus callosum, which was prevented by PARP inhibitor (**Fig. 23a-c**). In contrast, cuprizone did not induce caspase-dependent cell death as revealed by absence of procaspase-3 cleavage determined by immunoblotting, and a fluorescent caspase-3 assay (data not shown). Taken together, these data indicate caspase-independent AIF-mediated cell death in the corpus callosum of cuprizone-fed mice.

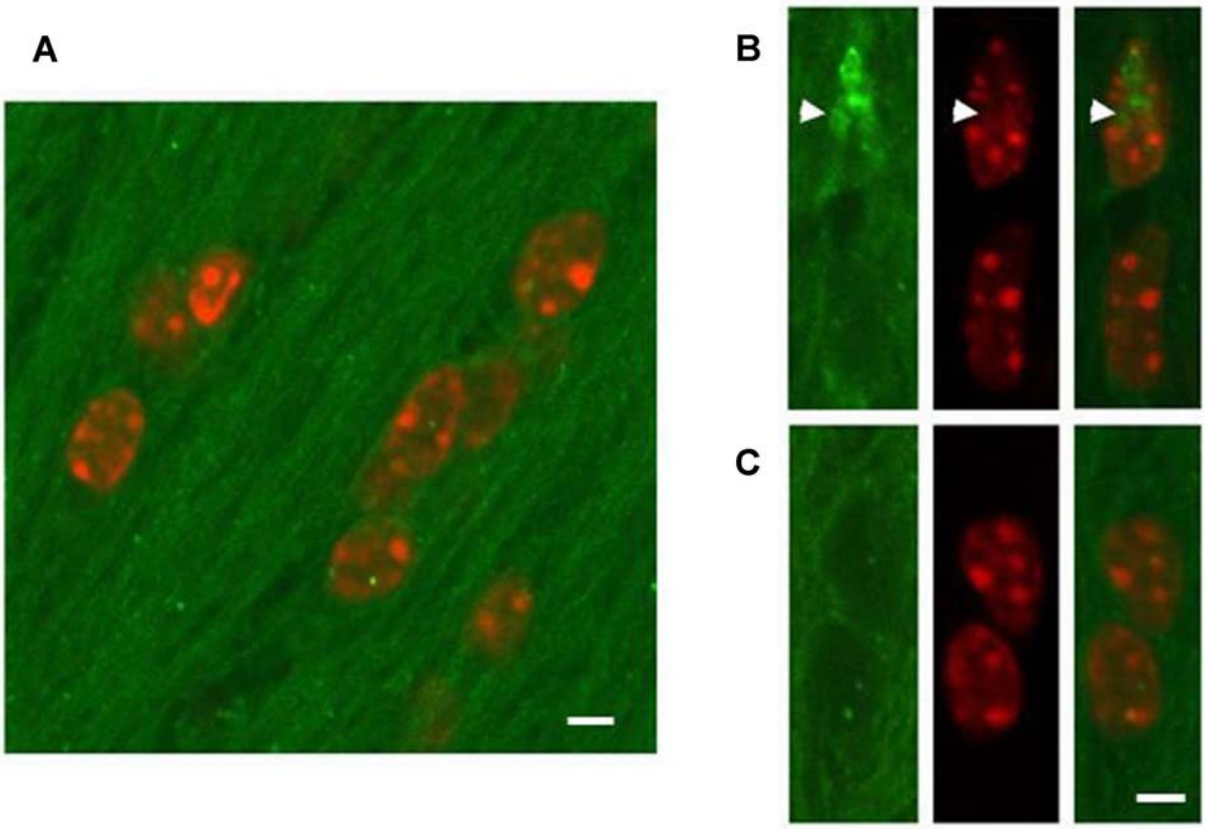


**Fig. 23 Effect of cuprizone and 4HQ on the nuclear translocation of AIF in the corpus callosum.** For demonstration of its nuclear translocation, AIF (green) immunohistochemisty with PI nuclear counterstaining (red) was performed, and confocal microscopy images were taken from representative areas of the midline of the corpus callosum of mice treated for three weeks. Photomicrographs were taken using a 60x oil immersion objective. Experiments were repeated three times and at least five mice were included in each group in all experiments.
(**a**) Representative merged image of untreated control mice (scale bar: 10 μm).
(**b** and **c**) Representative images of the green channel (left panels), the red channel (middle panels) and merged channels (right panels) of cuprizone (**b**) and cuprizone+4HQ (**c**) treated mice. Arrowheads indicate a cell where nuclear translocation of AIF occurred (scale bar: 10 μm).

### 4.3.3 Cuprizone treatment activated MAP kinases in the corpus callosum, which was modulated by PARP inhibition

Three weeks of cuprizone feeding induced activation of the MAP kinases, i.e. JNK, p38-MAPK and ERK1/2 ($p<0.01$, respectively) indicated by immunoblotting utilizing phosphorylation-specific primary antibodies (**Fig. 24**). 4HQ treatment attenuated cuprizone-induced phosphorylation of JNK, and p38-MAPK significantly

(p<0.01 and p<0.05, respectively) but not of ERK1/2. In contrast, 4HQ alone did not affect phosphorylation of the MAP kinases (**Fig. 24**).

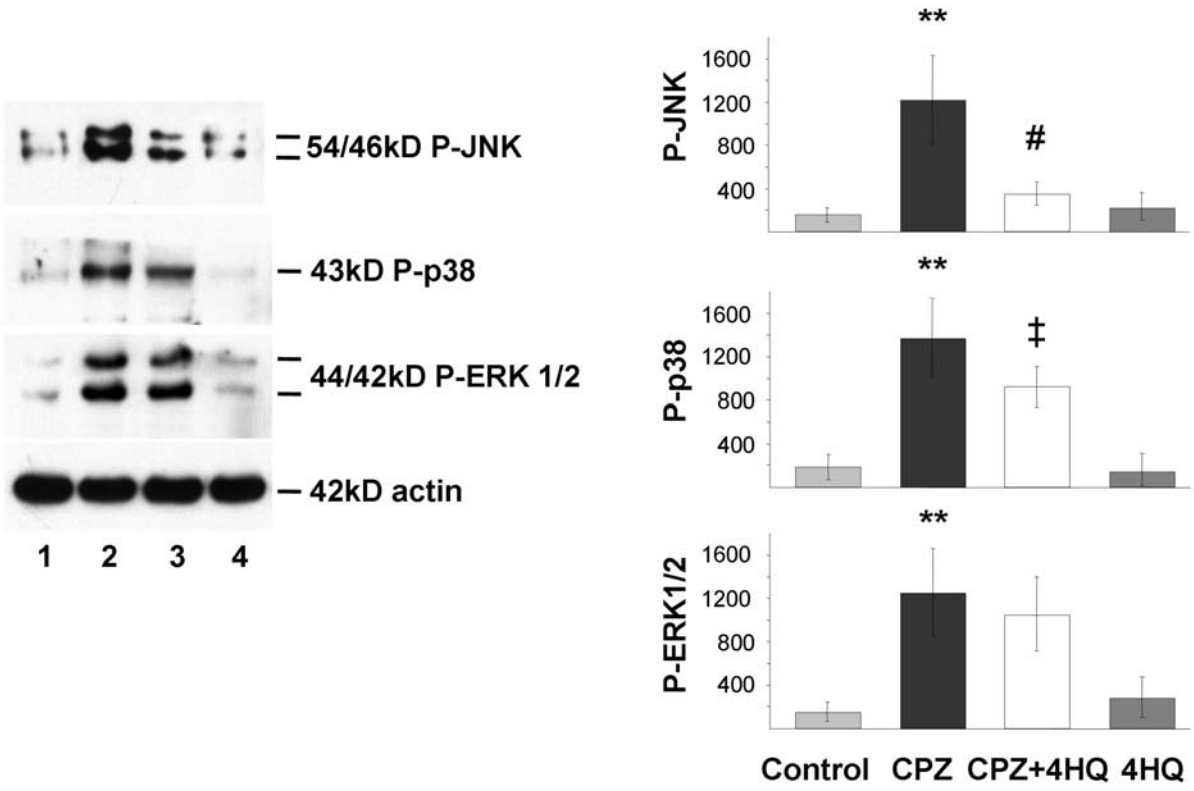


**Fig. 24 Effect of cuprizone and 4HQ treatment on the phosphorylation state of mitogen-activated protein kinases in the corpus callosum.** Representative immunoblot from three experiments (at least five mice in each group) (left panel) and densitometric evaluations (right panel) are shown. MAPK phosphorylation in the dissected corpus callosum of mice treated for three weeks was detected by immunoblotting utilizing phosphorylation-specific antibodies (P-Thr$^{180}$/Tyr$^{182}$-p38-MAPK, P-Thr$^{183}$/Tyr$^{185}$ -JNK, P-Thr$^{183}$/Tyr$^{185}$- ERK1/2). Even protein loadings were confirmed by anti-actin antibody and immunoblotting.
*Lane 1*, control; *lane 2*, cuprizone (CPZ) treatment*; lane 3*, cuprizone and 4HQ (CPZ+4HQ) treatment; *lane 4*, 4HQ treatment. Results on diagram are expressed as mean pixel densities ±SD; **p<0.01 compared to control; ‡p<0.05 compared to cuprizone group; #p<0.01 compared to cuprizone group.

### 4.3.4 Cuprizone treatment activated Akt in the corpus callosum, which was further enhanced by PARP inhibition

Three weeks of cuprizone feeding induced activation of Akt in the corpus callosum indicated by immunoblotting utilizing a phosphorylation-specific primary antibody (p<0.05, **Fig. 25**).

In contrast to the effect on MAP kinases, 4HQ enhanced cuprizone-induced phosphorylation of Akt ($p<0.05$). In addition, PARP inhibition alone also resulted in increased phosphorylation of Akt ($p<0.05$, **Fig. 25**).

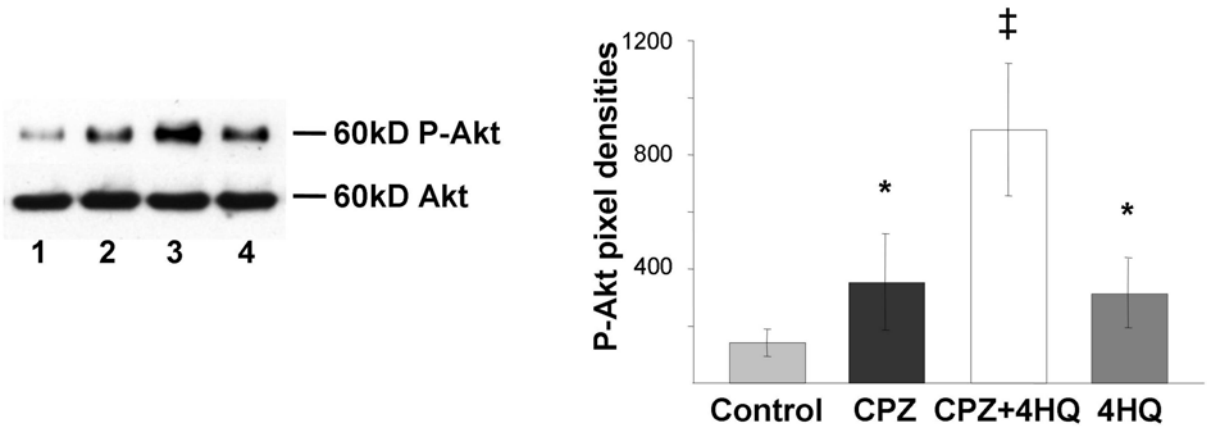


**Fig. 25 Effect of cuprizone and 4HQ treatment on the phosphorylation state of Akt in the corpus callosum.** Representative immunoblots from three experiments (at least five mice in each group) (left panel) and densitometric evaluations (right panel) are shown. Akt phosphorylation in the dissected corpus callosum of mice treated for three weeks was detected by immunoblotting utilizing phosphorylation-specific Akt antibody (P-Ser$^{473}$ Akt). Even protein loadings were confirmed by anti-Akt antibody and immunoblotting.
*Lane 1*, control; *lane 2*, cuprizone (CPZ) treatment*; lane 3*, cuprizone and 4HQ (CPZ+4HQ) treatment; *lane 4*, 4HQ treatment. Results on diagram are expressed as mean pixel densities ±SD; *$p<0.05$ compared to control; ‡$p<0.05$ compared to cuprizone group.

## 5. DISCUSSION

### 5.1 Effects of PARP inhibition on weight loss, hydrocephalus formation and demyelination induced by cuprizone

In the first part of our study, we used cuprizone-induced demyelination as an animal model for oligodendrocyte depletion, the main characteristic of multiple sclerosis and showed the protective effect of PARP inhibition in this model.

Demyelination and oligodendrocyte death is one of the general features of multiple sclerosis, which has even been suggested to be the primary event in lesion evolution, may contribute to chronic inflammation through epitope spreading and axonal degeneration, which correlates with clinical disability [Naismith and Cross,2005]. Alternatively, oligodendrocyte injury and tissue destruction may be the consequence of the inflammatory process of MS [Lassmann et al.,2007; Smith and Lassmann,2002]. Irrespective of the primary trigger for oligodendrocyte death in MS, mitochondrial dysfunction with subsequent apoptotic cell death is a cardinal feature in at least a subset of acute and chronic MS lesions [Aboul-Enein et al.,2003; Mahad et al.,2008] and this feature is shared between the cuprizone model and MS.

The administration of a toxin, cuprizone (bis-cyclohexanone-oxaldihydrazone) to young adult mice induces a consistent demyelination of the corpus callosum, superior cerebellar peduncle [Matsushima and Morell,2001], besides basal ganglia, cerebellar and cerebral cortex [Gudi et al.,2009; Pott et al.,2009; Skripuletz et al.,2010]. Upon cuprizone administration mature oligodendroglia are specifically insulted and go through apoptosis, without damage to other cell types in the central nervous system other than oligodendrocytes [Blakemore W,1972; Komoly et al.,1987; Ludwin,1978; Matsushima and Morell,2001; Pattison and Jebbett,1971]. This is closely followed by recruitment of microglia and phagocytosis of myelin, demyelination [Matsushima and Morell,2001], whereas T cells are almost completely absent during demyelination events [Hiremath et al.,1998] that may be related to the presence of an intact blood-brain barrier (BBB) [Bakker and Ludwin,1987; Kondo et al.,1987].

Cuprizone is a copper chelator originally produced for use in clinical chemistry, and in the brain and liver of animals dosed with this substance leads to inhibition of the copper-dependent mitochondrial enzymes cytochrome oxidase and monoamine

oxidase [Hoppel and Tandler,1973; Venturini,1973]. Deficiency in the activity of a crucial component of oxidative phosphorylation, the copper requiring mitochondrial electron carrier, cytochrome oxidase makes plausible the hypothesis that disturbance in energy metabolism leads to apoptosis in the oligodendrocytes, which causes demyelination. Decreased activity of the respiratory chain enzymes could also be detected in cultured oligodendrocytes *in vitro* [Pasquini et al.,2007]. Moreover, the first event of cuprizone intoxication is the formation of megamitochondria (enlargement or clustering) in hepatocytes and in oligodendrocytes [Suzuki and Kikkawa,1969; Suzuki,1969; Venturini,1973], thus emphasizing the role of mitochondrial dysfunction in this model. Enlargement of mitochondria could also be detected in cultured oligodendrocytes treated with cuprizone [Cammer,1999].

Impaired functioning of the mitochondrial respiratory chain leads to formation of excessive amount of ROS [Turrens,2003] as measured *in vitro* in cuprizone treated cultured oligodendrocytes [Pasquini et al.,2007] that can contribute to megamitochondria formation and induction of apoptosis [Karbowski et al.,1999].

Oligodendrocytes are mature glial cells that myelinate axons in the brain and spinal chord. They are the end product of a cell lineage which has to undergo a complex and precisely timed program of proliferation, migration, differentiation, and myelination to finally produce the insulating sheath of axons. Due to this complex differentiation program, and due to their unique metabolism/physiology, oligodendrocytes count among the most vulnerable cells of the central nervous system [Bradl and Lassmann,2010].

It has been estimated that during the peak of myelination, oligodendrocytes elaborate about three times their weight in membrane per day, and eventually support membrane up to 100x the weight of their cell body [Ludwin,1997; Mclaurin and Yong,1995; McTigue and Tripathi,2008]. This particular feature renders oligodendrocytes vulnerable at several different ‘‘Achilles’ heels’’.

First, in order to myelinate properly, oligodendrocytes must have extremely high metabolic rates, and must consume large amounts of oxygen and ATP [McTigue and Tripathi,2008]. The production of ATP in the mitochondria leads to the formation of ROS as toxic by-products, and a high cellular metabolism creates large amounts of ROS, which must be properly metabolized [McTigue and Tripathi,2008]. Second, myelination is under control of many myelin synthesizing enzymes, which require iron

as a co-factor [Connor and Menzies,1996; Todorich et al.,2009]. This may contribute to the observation that oligodendrocytes have the largest intracellular stores of iron in the brain [Thorburne and Juurlink,1996; Todorich et al.,2009], which can, under unfavourable conditions, evoke free radical formation and lipid peroxidation [Braughler et al.,1986; Juurlink,1997]. On top of this, oligodendrocytes contain only low concentrations of the anti-oxidative peptide glutathione [Juurlink et al.,1998; Thorburne and Juurlink,1996]. Due to the combination of a high metabolic rate with its toxic by-products, high intracellular iron, and low concentrations of the antioxidative glutathione, oligodendrocytes are particularly vulnerable to oxidative damage and mitochondrial injury [Ghafourifar et al.,2008; Jana and Pahan,2007]. This is probably reflected by the profound oligodendrocyte damage in certain toxic states which interfere with mitochondrial function and it could be the reason why oligodendrocytes undergo selective apoptosis in the brain upon cuprizone administration.

Since mitochondrial dysfunction results in excessive ROS production which could lead to DNA breakage and PARP activation [Schreiber et al.,2006] promoting cell death by ATP depletion and by regulating the release of AIF from mitochondria [Alano et al.,2004; Yu et al.,2002], we hypothesized that PARP activation plays a key role in the apoptosis of oligodendrocytes upon cuprizone treatment. Apoptotic oligodendrocytes are to be detected in the corpus callosum between two and four weeks of cuprizone treatment, reaching the peak on the third week of treatment, just prior to onset of demyelination [Matsushima and Morell,2001], therefore we performed anti-PAR immunohistochemistry and immunoblotting on corpus callosum after three weeks of cuprizone administration to investigate PARP activity.

At this time point anti-PAR immunohistochemistry and immunofluorescence revealed very strong PAR reactivity, although not in every, but in apoptotic oligodendrocytes. Also PAR immunoblotting of the whole corpus callosum showed elevated PAR levels. Poly(ADP-ribose) (PAR) is the product of PARP and its breakdown is mediated by poly(ADP-ribose)glycohydrolase (PARG), an enzyme with both exo- and endoglycosidase activities that hydrolyses the glycosidic bond between ADP-ribose units. Its predominant isoforms are the very active nuclear PARG protein and a short mitochondrial isoform [Schreiber et al.,2006]. An alternative pathway for PAR degradation is PAR hydrolysis mediated by ADP-

ribosylarginine hydrolase-3 [Oka et al.,2006]. This indicates the complexity of PAR metabolism and makes clear that the amount of PAR is not equal to PARP activity, rather reflects a steady state level which depends on mechanisms of PAR formation and breakdown. Still, strongly increased PAR levels in dying oligodendrocytes of the corpus callosum after three weeks of cuprizone exposure may be suggestive of a highly increased PARP activity supporting our hypothesis.

In order to investigate the possible protective effect of PARP inhibition on oligodendrocytes, we examined the myelination status of the corpus callosum, the most studied area affected by cuprizone-induced demyelination.

Therefore, we first performed sequential $T_2$-weighted MRI in a weekly manner and found significant hyperintensities in the corpus callosum, suggesting a marked change of microstructure, corresponding to demyelination [Merkler et al.,2005] after four weeks of cuprizone treatment which became less prominent during the last two weeks. This is in agreement with ultrastructural studies, revealing that a substantial demyelination of the corpus callosum is present at the third week of treatment and by the fourth-fifth week more than 90% of the axons are demyelinated, whereas by the end of the sixth week of treatment and in spite of the continued exposure to cuprizone, there is recovery so that about 50% of the axons are again myelinated, remyelination occurs [Matsushima and Morell,2001]. It is assumed that spontaneous remyelination takes place because of proliferation and differentiation of either local or recruited oligodendrocyte progenitor cells. Co-administration of 4HQ, a potent PARP inhibitor with cuprizone reversed the appearance of hyperintensities indicating preserved myelin throughout the whole experiment.

After five weeks of treatment we also assayed corpus callosum with myelin staining luxol fast blue (LFB) histochemistry. It revealed severe myelin loss in the corpus callosum, in accordance with other studies, where by means of LFB staining the peak of demyelination in the corpus callosum occurred after 4.5 weeks of cuprizone treatment [Gudi et al.,2009]. Co-treatment with 4HQ resulted in partial myelin protection as shown by LFB staining.

Myelin basic protein is one of the proteins that make up myelin and is expressed by oligodendrocytes. Its amount correlates well with the amount of myelin. After five weeks of treatment we performed quantification of the myelin status of the dissected corpus callosum by MBP immunoblotting and found a significantly decreased MBP

level. This was again in agreement with observations that revealed maximal loss of MBP after 4.5 weeks of cuprizone exposure [Gudi et al.,2009; Jurevics et al.,2002]. Similarly to the observations by LFB staining, when animals were co-treated with PARP inhibitor the observed MBP levels were significantly higher than in cuprizone only treated animals indicating myelin protecting effect of PARP inhibition.

In summary, intraperitoneal administration of 4HQ, a potent PARP inhibitor attenuated demyelination of the corpus callosum as we observed by means of MRI, histopathology and MBP immunoblotting. Specificity and possible side-effects of a pharmacological agent is always an issue. However, 4HQ was reported to have a high potency on PARP-1 and no effects on enzymes other than PARP have been documented [Banasik et al.,1992]. Moreover, PAR-immunoblotting of the dissected corpus callosum showed significantly lower PAR levels upon 4HQ co-treatment when compared to the levels of cuprizone treated. 4HQ decreased also the base-line levels of PAR in the corpus callosum, when mice were only 4HQ-treated. Since cuprizone leaves the BBB intact [Bakker and Ludwin,1987; Kondo et al.,1987], it could be assumed that 4HQ can penetrate the BBB. Small molecules generally cross the BBB in pharmacologically significantly amounts if 1) the molecular mass of the drug is less than 400-500 Da, and 2) the drug forms less than 8-10 hydrogen bonds with solvent water [Pardridge,2007]. The molecular mass of 4HQ is 146 Da, and it can form maximum four hydrogen bonds, supporting the hypothesis that 4HQ is able to go through the BBB. Therefore, it seems likely that diminished demyelination induced by cuprizone can be assigned to the PARP inhibitory effect of 4HQ.

Similar to oligodendrocytes, hepatocytes have also been shown to develop megamitochondria upon cuprizone treatment indicating mitochondrial dysfunction [Suzuki and Kikkawa,1969]. Therefore, malfunctioning of mitochondrial respiratory chain and concomitant disturbance of energy metabolism could also explain the systemic effect of cuprizone, weight loss. In accordance with previous findings [Carlton,1966; Hoppel and Tandler,1973], we found a continuous decrease in body mass of mice during the six weeks of cuprizone treatment. An interesting question could have been, whether the weight loss was accompanied with an increased, decreased or normal food intake, and how cuprizone influenced the metabolism of mice. Since mice received cuprizone mixed in with powdered chow placed in the cage in Petri dish, the animals could disperse it easily which made it technically

difficult to measure the daily consume of feed. Besides, the aim of the weekly measurement of body mass was simply to follow the effect of cuprizone intoxication. Nevertheless, we found that PARP inhibition could anti-dote this weight decreasing effect of cuprizone. PARP activity results in diminished intracellular levels of $NAD^+$ inhibiting efficient synthesis of ATP, hence PARP inhibition could contribute to the restoration of sufficient cell energy metabolism explaining the protective effect against weight loss.

Another feature of this animal model for demyelination is that mice develop hydrocephalus [Carlton,1966; Carlton,1967]. Early experiments in the cuprizone model reported mild stenosis of the aqueduct of Sylvius and microscopic hydrocephalus by the end of two weeks of cuprizone administration, but it was not until the end of third week of feeding that definite stenosis of the aqueduct occurred and gross hydrophalus was evident [Kesterson and Carlton,1970]. Since the first pathological change observed in their sequential study was edema of the mesencephalon and diencephalon, Kesterson and Carlton suggested that stenosis resulted from the compression of the anatomically narrow aqueduct by edematous midbrain tissue followed by hydrocephalus development from continuous normal secretion of the liquor cerebrospinalis. In the present study we did not investigate mechanisms underlying hydrocephalus formation but follow its development by weekly sequential MR imaging of the brains. Since the brain and ventricles of weanling mice can change in size as mice grow, we determined the extent of hydrocephalus by means of calculating ventricle volume/ brain volume ratios. Different from previous findings [Kesterson and Carlton,1970], quantification revealed significantly higher ratios only after four weeks of cuprizone treatment. However, it is important to note that Kesterson and Carlton administered cuprizone to Swiss albino mice and in higher doses (0.3 m/m%) which could explain the earlier development of hydrocephalus. Moreover, estimations of hydrocephalus via histology are not reliable, since tissues of the brain and therefore ventricles can shrink due to fixation processes leading to false results. This was the first time when hydrocephalus formation upon cuprizone treatment was evaluated by means of MR imaging and quantification was carried out.

BBB upon cuprizone administration has been shown to remain intact [Bakker and Ludwin,1987; Kondo et al.,1987] hence the edema described by Kesterson and

Carlton is reminiscent of cytotoxic cerebral edema. Cytoxotic edema is seen with various intoxications, in acute liver and kidney failure, early hypoxia or ischemia [Nag et al.,2009]. Its formation is due to the derangement in cellular metabolism resulting in inadequate functioning of the sodium and potassium pump in the glial cell membrane. As a result there is cellular retention of sodium and water and astrocytes are swollen [Nag et al.,2009]. The disturbed energy metabolism caused by cuprizone could readily result in the formation of cytotoxic edema.

In addition, we found that PARP inhibition prevented cuprizone induced hydrocephalus development throughout the whole experiment that could be explained again by the cell energy metabolism restoring effect of PARP inhibition.

In summary, we can say that although we showed PARP activation only in the corpus callosum, administration of the PARP inhibitor 4HQ anti-doted not only the demyelinating effect of cuprizone but prevented also formation of hydrocephalus and weight loss indicating that PARP inhibition influenced not only oligodendrocyte-specific but more general effects of cuprizone.

### 5.2 Effects of cuprizone and PARP inhibition on thymi of mice

In the second part of our study, we investigated changes of the thymus upon cuprizone intoxication and found severe atrophy of the organ due to apoptosis of thymocytes $CD4^+CD8^+$ double positive thymocytes being the mostly affected and revealed also the disruption of the thymic stroma. Moreover, we showed the protective effect of PARP inhibition against cuprizone-induced acute thymic involution.

Thymus is a vital organ for homeostatic maintenance of the peripheral immune system, and undergoes a continuous age-associated change in structure and cell constitution, leading to age-related thymic involution and less efficient T-cell development [Lynch et al.,2009]. In case of mice, most of the thymocytes of 15-day-old foetuses are of DN phenotype, whereas the majority of the thymocytes of newborn mice are DP [Oh and Kim,1999]. With advancing age, there is a well-described loss of maturing DP thymocytes, loss of total thymocyte number and shrinkage of thymic tissue [Lynch et al.,2009; Sempowski et al.,2002]. Since thymic involution occurs soon after birth [Sempowski et al.,2002], we chose to treat 4-week-

old mice for one week to investigate the effects of cuprizone on thymocytes. According to the literature, 4-week-old C57BL/6 mice have a mean thymus weight of 60 mg and an absolute thymocyte number of about $80x10^6$ [Hick et al.,2006]. In concert with these data, we found in 5-week-old control mice a mean thymus mass of 60 mg, and a mean thymocyte number of $65x10^6$. In young adult mice the ratios of the different thymocyte populations are generally 5% for DN, 70-85% for DP and 15% for SP T cells with a $CD4^+/CD8^+$ SP ratio of 2:1 [Oh and Kim,1999; Savino et al.,2007]. Similarly, in 5-week-old C57BL/6 male control animals we found 9.81% DN, 73.37% DP, 11.56% $CD4^+$ SP and 5.25% $CD8^+$ SP ratio of the whole thymocyte population. As 5-week-old mice are in about weanling age, the about two times higher ratio of DN cells could be explained by the earlier stage in thymic development.

Upon cuprizone treatment we observed massive atrophy of the thymus with decrease in thymus/whole body mass ratio and thymocyte number. AnnexinV/PI flow cytometry of the remaining thymocytes indicated that thymocytes died by apoptosis and living thymocytes showed marked change in the ratios of the thymocyte subpopulations. An almost total disappearance of the $CD4^+$ $CD8^+$ DP population was observed with concomitant and about equal increase of the DN and SP populations, suggesting that although there was a massive decrease in the number of the DN, and SP thymocytes too but it was the DP population that proved to be the most susceptible to the cuprizone challenge, DN and SP populations were less and about equally affected. Consequently, we did not find any change in the $CD4^+$ SP/$CD8^+$ SP ratio that could have explained the decreased $CD4^+$ SP/$CD8^+$ SP ratio in the blood upon two weeks of cuprizone treatment described by Emerson and co-workers [Emerson et al.,2001]. Moreover, contrary to their observations, in our preliminary study we could not find any change in the $CD4^+$ SP/$CD8^+$ SP ratio in the blood of mice after one week of cuprizone treatment when compared to control (*data not shown*) but further investigations are needed.

Thymus undergoes physiologic involution due to aging, but also undergoes pathologic atrophy induced by a variety of causes, including infectious diseases, sepsis, malnutrition, physical or emotional stress, chemotherapeutics, glucocorticoids or radiation injury [Dal-Zotto et al.,2003; Engler and Stefanski,2003; Gruver and Sempowski,2008; Hick et al.,2006; Kioukia-Fougia et al.,2002; Schuurman et

al.,1994; Wang et al.,1994]. In these cases, atrophy is a result of the massive apoptosis of cortical DP cells, whereas $CD4^+$ or $CD8^+$ SP cells are less affected [Grillot et al.,1995; Pearse,2006; Savino et al.,2007; Strasser et al.,1991]. In addition, during physiological thymic development, positive and negative selection, roughly 98% of $CD4^+CD8^+$ DP thymocytes undergo apoptosis before maturing to the $CD4^+$ or $CD8^+$ SP stage. It is therefore well established that DP thymocytes are more sensitive to myriad death stimuli, apoptosis inducing factors, physiological and pathological conditions than $CD4^+$ or $CD8^+$ SP thymocytes. It is assumed that mitochondria in DP thymocytes are more primed for death than those in SP, as they are loaded with pro-death proteins of the BCL-2 family (Bax, Bak) that are required for MOMP or with activator or sensitizer proteins of the BCL-2 family (Bid, Bim) and can therefore enter the intrinsic or mitochondrial pathway of apoptosis at a lower threshold of pro-death signalling (**Fig. 3**) [Ryan et al.,2010].

Since cuprizone induces mitochondrial dysfunction with concomitant ROS production, it is probable that cells with primed mitochondria are more vulnerable to this cell death trigger. Thymocyte apoptosis-inducing effect of cuprizone could be also a result of either direct immunotoxicity or of a secondary immunosuppression via stress-elevated glucocorticoid hormone levels similarly to many above mentioned pathological settings such as undernutrition [Chandra,1999], physical and emotional stress [Dal-Zotto et al.,2003; Engler and Stefanski,2003], infection [Hick et al.,2006] and sepsis [Wang et al.,1994]. Since we observed a significant weight loss of mice and assumed a general energy deficiency in the background of it, this might imply a general stress reaction upon cuprizone treatment with elevated glucocorticoid levels similar to undernutrition.

On the other hand, in different settings of copper deficiency reduced T cell response was observed with significantly lower thymus weights resulting from reduction in the concentration of interleukin-2 (IL-2) [Hopkins and Failla,1995; Koller et al.,1987; Lukasewycz and Prohaska,1990; Prohaska et al.,1983]. Although IL-2 is known to play an important role in terminal differentiation of effector cells in primary responses, aspects of memory recall responses and thymic development of regulatory T cells [Malek and Castro,2010], it has been suggested that the immunosuppressant cyclosporine A exerts its lymphotoxic affect through inhibiting IL-2 transcription [Stepkowski,2000] resulting in prevention of peripheral T cell activation, in the thymus inhibition of positive selection, thymocyte loss and thymic

atrophy [Huby et al.,1995; Urdahl et al.,1994]. It is now well established that copper is necessary for transcription of IL-2 in T-lymphocytes [Bala and Failla,1992; Hopkins and Failla,1999]. As cuprizone acts as a copper chelator the observed thymic pathology could also be likely due to lowered IL-2 levels. To further elucidate thymocyte depleting effect of cuprizone, assessment of IL-2 and glucocorticoid levels are to be performed.

Besides thymocyte loss, we found a general decrease in cellularity of the thymic epithelial cells with loss of the sponge-like structure upon cuprizone treatment. Both cTEC and mTEC were affected with thinning of the stromal cortex and disappearance of the stromal medulla. Similarly to our observations, it has been described in mice treated with the immunosuppressants cyclophosphamid and dexamethasone that parallel to the decrease in thymocyte number extensive loss of total TECs occurred too [Fletcher et al.,2009]. The bi-directional symbiosis between thymocytes and stromal cells makes it always difficult to ascertain whether these immunosuppressive agents directly affect TEC survival or act through the depletion of thymocytes, however the fact that DP cells are primed for apoptosis and TEC do not express IL-2 receptor argue for the latter possibility.

Though mechanisms behind thymocyte apoptosis and TEC depletion upon cuprizone treatment are not yet understood, administration of the PARP inhibitor could prevent thymic atrophy as indicated by determination of thymic mass, relative mass and absolute thymocyte number. In previous studies increased PARP activity was described in thymocytes in nitroxyl-induced oxidative stress and MNNG-induced cytotoxicity [Bai et al.,2001; Bai et al.,2007]. Moreover, PARP inhibitors could partially protect thymocytes from cell death in these settings [Bai et al.,2001; Bai et al.,2007]. Presuming that cuprizone induces excessive ROS production also within thymocytes, it could be assumed that PARP inhibition protected thymocyte again against oxidative stress induced cell death.

### 5.3 Mechanisms underlying cuprizone induced oligodendrocyte death and its prevention by PARP inhibition

In the last part of our study we investigated the underlying mechanisms of cuprizone-induced demyelination and of the protective effect of PARP inhibition in the corpus callosum.

As discussed earlier cuprizone-induced mitochondrial dysfunction with excessive ROS production suggested by previous studies [Pasquini et al.,2007; Turrens,2003] could cause PARP activation [Schreiber et al.,2006], which we demonstrated by PAR-immunoblotting and immunohistochemistry. Overactivation of PARP promotes cell death by ATP depletion in the cell and by regulating the release of AIF from mitochondria [Alano et al.,2004; Yu et al.,2002]. AIF then translocates to the nucleus, leading to chromatin condensation, large-scale DNA fragmentation (>50 kbp) and cell death in a caspase-independent manner [Jurewicz et al.,2005; Lorenzo and Susin,2004]. In pattern III MS lesions we observed earlier strong PAR positivity in oligodendrocytes showing morphological features of apoptosis, moreover nuclear translocation of AIF co-localized with PAR positivity in several oligodendrocytes could be detected [Veto et al.,2010]. Furthermore, in early lesions the apoptosis of oligodendrocytes was found to be activated caspase 3 independent [Barnett and Prineas,2004]. Similar to this in the present study, we showed nuclear translocation of AIF in the cuprizone model which could not be detected when the PARP inhibitor was co-administered. However, we were unable to detect caspase-3 activation either by fluorescent caspase-3 substrate or by cleavage of pro-caspase-3 detected by immunoblotting (*data not shown*) in the corpus callosum of cuprizone-treated mice in agreement with previous findings [Copray et al.,2005; Pasquini et al.,2007], suggesting a caspase-independent, AIF-mediated cell death mechanism of dying oligodendrocytes underlying the similarities between the cuprizone model and MS.

JNK and p38-MAPK activation is considered to promote oligodendrocyte cell death [Ha et al.,2002; Jurewicz et al.,2003; Stariha and Kim,2001; Xia et al.,1995]. Indeed, we observed that cuprizone increased phosphorylation of JNK and p38-MAPK in the corpus callosum that was attenuated upon PARP inhibition, which is in agreement with previous findings, where PARP induced JNK activation was necessary for PARP activity triggered MOMP and AIF translocation [Xu et al.,2006]. Cuprizone-induced ERK1/2 activation in the corpus callosum as well, but it was not

affected by the PARP inhibitor 4HQ, which can be explained by the notion that MAPK/ERK kinase-ERK1/2 pathway is upstream to PARP activation [Kauppinen et al.,2006; Tang et al.,2002]. Since ERK activation was found to promote oligodendrocyte survival [Cohen et al.,1996; Yoon et al.,1998], cuprizone-induced ERK activation may represent a compensatory protective mechanism against oligodendrocyte death. On the other hand, it has also been suggested that for a maximal PARP activation after DNA damage phosphorylation of the enzyme by ERK2 is required [Kauppinen et al.,2006], therefore upon cuprizone treatment the enhanced ERK activity may rather contribute to cell death signalling. In conclusion, effects of PARP inhibition on the MAPK pathways, i.e. suppressing JNK and p38 activation while not affecting ERK, could promote oligodendrocyte survival leaving the role of ERK undetermined (**Fig. 26**).

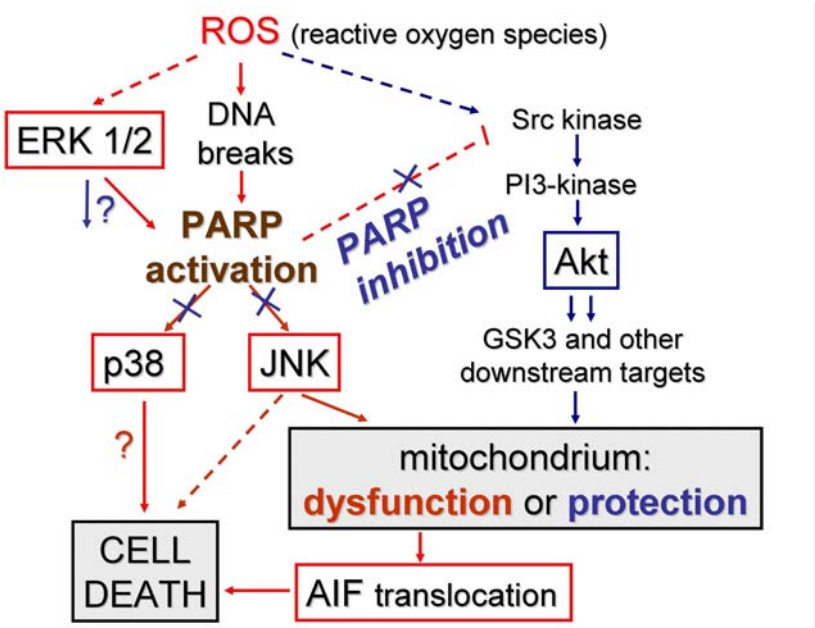


**Fig. 26 Possible mechanisms of PARP inhibition on cuprizone-induced apoptosis.** The protective effect of 4HQ is mediated by attenuating MAP-kinase-dependent cell death and nuclear translocation of AIF as a result of mitochondrial damage (red). Enhanced activation of Akt may provide additional protection against mitochondrial oligodendrocyte death (blue) as it is indicated on this scheme.

Cuprizone intoxication also resulted in Akt activation (i.e. phosphorylation), which was further enhanced by co-administration of 4HQ. Furthermore, PARP inhibition alone caused enhanced phosphorylation of Akt in accordance with previous findings [Tapodi et al.,2005; Veres et al.,2003]. Activation of Akt prevented neuronal apoptosis by inhibiting translocation of AIF to the nucleus [Kim et al.,2007], protected oligodendrocytes against TNF-induced apoptosis [Pang et al.,2007] and by

phosphorylating their respective upstream kinases, decreased activity of JNK and p38-MAPK [Barthwal et al.,2003; Park et al.,2002]. Based on these data, our results may suggest that in response to cuprizone, the cytoprotective PI-3K/Akt pathway became activated, although was insufficient to prevent oligodendrocyte death. Additional activation by PARP inhibition could be sufficient to protect oligodendrocytes against apoptosis, mediated partially by reduced activation of JNK and p38-MAPK and maintaining the integrity of the mitochondrial membrane systems preventing MOMP and nuclear translocation of AIF (**Fig. 26**).

## 6. SUMMARY AND CONCLUSIONS

In our study we investigated an animal model of demyelination and oligodendrocyte depletion, as observed in multiple sclerosis. The mitochondrial toxin, cuprizone induces besides the selective apoptosis of oligodendrocytes also formation of hydrocephalus and weight loss in weanling C57BL/6 male mice [Hiremath et al.,1998]. We showed enhanced PARP activation in the most demyelinated brain area, corpus callosum upon cuprizone treatment. Administration of 4HQ, a potent PARP inhibitor decreased the PARP activity and prevented demyelination as demonstrated by MRI, histopathology and myelin basic protein immunoblotting. PARP inhibition protected mice also from other effects of cuprizone, i.e. from development of hydrocephalus and severe weight loss.

Besides these known effects of cuprizone, we described at the first time that cuprizone administration to 4-week-old male mice resulted in severe thymic atrophy even after one week. We demonstrated that thymocytes died by apoptosis and found $CD4^+$ $CD8^+$ DP thymocytes the most vulnerable. Also, we revealed the disruption of the thymic stroma too. Changes of the thymus could explain the attenuated T cell response after cuprizone intoxication described by Emerson and co-workers.

Moreover, we showed that PARP inhibition protected mice from acute thymic involution. Acute thymic involution and concomitant impaired peripheral immune response is a complication of malnutrition, infections, sepsis or other stress events. Since PARP inhibition showed promising results in preventing cuprizone induced thymic atrophy and as there are currently no treatments available to protect against acute thymic involution or accelerate recovery leaving the immune system compromised during acute stress, further investigations in this topic could be of great importance.

We also intended to elucidate the underlying molecular mechanisms of cuprizone induced oligodendrocyte apoptosis and found besides PARP activation elevated AIF expression, AIF nuclear translocation and revealed no caspase-3 activation. Moreover, we detected increased phosphorylation levels of the MAP kinases, i.e. ERK1/2, p38 MAPK, and JNK and of the cytoprotective Akt/PKB upon cuprizone treatment in the corpus callosum. PARP inhibitor co-treatment decreased elevated AIF expression, prevented AIF nuclear translocation and attenuated the activation of

JNK and p38, which are usually known to play a role in apoptosis and inflammation. Besides, PARP inhibition enhanced further the phosphorylation of Akt contributing to the cell protecting effect of 4HQ.

In the cuprizone model of demyelination, the observed patterns of at least two key molecular mechanisms, i.e. PARP activation and caspase-independent AIF-mediated apoptosis of oligodendrocytes are identical in both pattern III MS lesions and cuprizone-induced demyelination [Veto et al.,2010]. Besides, cuprizone induced pathological changes are similar to pattern III lesions or MS lesions defined by Barnett and Prineas [Barnett and Prineas,2004; Lucchinetti et al.,2000]. Accordingly, the earliest change is wide-spread oligodendrocyte apoptosis associated with microglia activation in the proximity of dying oligodendrocytes, while signs of humoral and cellular immune responses are minor. Based on these pathological and molecular observations, it could be assumed that the apoptosis of oligodendrocytes at least in a subgroup of MS patients and in the cuprizone model happens via similar pathways. Thus, inhibition of PARP may be similarly effective in MS. By blocking demyelination, PARP inhibition may reduce inflammation through preventing epitope spreading. Besides, it also has a direct effect on inflammation indicated by reduced clinical signs of EAE [Scott et al.,2004]. Inhibiting PARP thus may influence degenerative and autoimmune inflammatory processes in MS and provide an effective therapy targeting two basic mechanisms at the same time.

## 7. ACKNOWLEDGEMENTS

First of all, I would like to thank my supervisors Prof. Ferenc Gallyas Jr., Ph.D., D.Sc. and Prof. Balázs Sümegi, Ph.D., D.Sc. for managing my work and giving support and useful advices. I thank to Zoltán Berente, Ph.D. for his excellent help to perform NMR measurements and all my colleagues at the Department of Biochemistry and Medical Chemistry for their help and assistance in the laboratory work.

I am grateful to Prof. Sámuel Komoly, M.D., Ph.D., D.Sc. and Prof. Zsolt Illés, M.D., Ph.D., D.Sc. for guidance and advices during my work and especially to Péter Ács, M.D. for performing the histological experiments at the Department of Neurology. I would also like to acknowledge Prof. Hans Lassmann, M.D., Ph.D., D.Sc. and Jan Bauer, M.D., Ph.D. at the Brain Research Institute, University of Vienna for their co-operation in investigating multiple sclerosis lesions.

I am really thankful to Péter Balogh, M.D., Ph.D., László Pálinkás, M.D., Ph.D., Ferenc Boldizsár, M.D., Ph.D. and Gergely Talabér, M.D., Ph.D. at the Department of Immunology and Biotechnology for giving advice and performing the flow cytometric measurements and immunofluorescence of thymi.

I thank Gábor Borgulya, M.D. for his great help he gave me during performing statistical analysis.

Finally, I express my warmest thanks to my parents, my husband, my children and my whole family for their love and encouraging support.

## 8. REFERENCE LIST


Aboul-Enein F, Rauschka H, Kornek B, Stadelmann C, Stefferl A, Bruck W, Lucchinetti C, Schmidbauer M, Jellinger K and Lassmann H, 2003. Preferential loss of myelin-associated glycoprotein reflects hypoxia-like white matter damage in stroke and inflammatory brain diseases. Journal of Neuropathology and Experimental Neurology 62, 25-33.

Alano CC, Ying WH and Swanson RA, 2004. Poly(ADP-ribose) polymerase-1-mediated cell death in astrocytes requires NAD(+) depletion and mitochondrial permeability transition. Journal of Biological Chemistry 279, 18895-18902.

Allman D, Sambandam A, Kim S, Miller JP, Pagan A, Well D, Meraz A and Bhandoola A, 2003. Thymopoiesis independent of common lymphoid progenitors. Nature Immunology 4, 168-174.

Alves NL, Huntington ND, Rodewald HR and Di Santo JP, 2009. Thymic epithelial cells: the multi-tasking framework of the T cell "cradle". Trends in Immunology 30, 468-474.

Anderson G and Jenkinson EJ, 2001. Lymphostromal interactions in thymic development and function. Nature Reviews Immunology 1, 31-40.

Anderson G, Lane PJL and Jenkinson EJ, 2007. Generating intrathymic microenvironments to establish T-cell tolerance. Nature Reviews Immunology 7, 954-963.

Bai P, Bakondi E, Szabo E, Gergely P, Szabo C and Virag L, 2001. Partial protection by poly(ADP-ribose) polymerase inhibitors from nitroxyl-induced cytotoxicity in thymocytes. Free Radical Biology and Medicine 31, 1616-1623.

Bai P, Hegedus C, Erdelyi K, Szabo E, Bakondi E, Gergely S, Szabo C and Virag L, 2007. Protein tyrosine nitration and poly(ADP-ribose) polymerase activation in N-methyl-N-nitro-N-nitrosoguanidine-treated thymocytes: Implication for cytotoxicity. Toxicology Letters 170, 203-213.

Bakker DA and Ludwin SK, 1987. Blood-brain-barrier permeability during cuprizone-induced demyelination - implications for the pathogenesis of immune-mediated demyelinating diseases. Journal of the Neurological Sciences 78, 125-137.

Bala S and Failla ML, 1992. Copper deficiency reversibly impairs DNA-synthesis in activated lymphocytes-T by limiting interleukin-2 activity. Proceedings of the National Academy of Sciences of the United States of America 89, 6794-6797.

Banasik M, Komura H, Shimoyama M and Ueda K, 1992. Specific inhibitors of poly(ADP-Ribose) synthetase and mono(ADP-ribosyl)transferase. Journal of Biological Chemistry 267, 1569-1575.

Barnett MH and Prineas JW, 2004. Relapsing and remitting multiple sclerosis: Pathology of the newly forming lesion. Annals of Neurology 55, 458-468.

Barthwal MK, Sathyanarayana P, Kundu CN, Rana B, Pradeep A, Sharma C, Woodgett JR and Rana A, 2003. Negative regulation of mixed lineage kinase 3 by protein kinase B/AKT leads to cell survival. Journal of Biological Chemistry 278, 3897-3902.

Boyd RL and Hugo P, 1991. Towards an integrated view of thymopoiesis. Immunology Today 12, 71-78.

Bradl M and Lassmann H, 2010. Oligodendrocytes: biology and pathology. Acta Neuropathologica 119, 37-53.

Braughler JM, Duncan LA and Chase RL, 1986. The involvement of iron in lipid-peroxidation - importance of ferric to ferrous ratios in initiation. Journal of Biological Chemistry 261, 282-289.

Callebaut I and Mornon JP, 1997. From BRCA1 to RAP1: A widespread BRCT module closely associated with DNA repair. Febs Letters 400, 25-30.

Cammer W, 1999. The neurotoxicant, cuprizone, retards the differentiation of oligodendrocytes in vitro. Journal of the Neurological Sciences 168, 116-120.

Carlton WW, 1966. Response of mice to the chelating agents sodium diethyldithiocarbamate, a-benzoinoxime, and biscyclohexanone oxaldihydrazone. Toxicology and Applied Pharmacology 8, 512-521.

Carlton WW, 1967. Studies on the induction of hydrocephalus and spongy degeneration by cuprizone feeding and attempts to antidote the toxicity. Life Sciences 6, 11-19.

Chandra RK, 1999. Nutrition and immunology: from the clinic to cellular biology and back again. Proceedings of the Nutrition Society 58, 681-683.

Cohen RI, Marmur R, Norton WT, Mehler MF and Kessler JA, 1996. Nerve growth factor and neurotrophin-3 differentially regulate the proliferation and survival of developing rat brain oligodendrocytes. Journal of Neuroscience 16, 6433-6442.

Compston A and Coles A, 2008. Multiple sclerosis. Lancet 372, 1502-1517.

Connor JR and Menzies SL, 1996. Relationship of iron to oligodendrocytes and myelination. Glia 17, 83-93.

Copray JC, Kust BM, Mantingh-Otter I and Boddeke HW, 2005. p75NTR independent oligodendrocyte death in cuprizone-induced demyelination in C57BL/6 mice. Neuropathology and Applied Neurobiology 31, 600-609.

Dal-Zotto S, Marti O and Armario A, 2003. Glucocorticoids are involved in the long-term effects of a single immobilization stress on the hypothalamic-pituitary-adrenal axis. Psychoneuroendocrinology 28, 992-1009.

de Murcia G, Schreiber V, Molinete M, Saulier B, Poch O, Masson M, Niergang C and de Murcia M, 1994. Structure and function of poly(ADP-ribose) polymerase. Molecular and Cellular Biochemistry 138, 15-24.

Denic A, Johnson A, Bieber A, Warrington A, Rodriguez M and Pirko I, 2010. The relevance of animal models in multiple sclerosis research. Pathophysiology doi:10.1016/j.pathophys.2010.04.004,

Emerson MR, Biswas S and Levine SM, 2001. Cuprizone and piperonyl butoxide, proposed inhibitors of T-cell function, attenuate experimental allergic encephalomyelitis in SJL mice. Journal of Neuroimmunology 119, 205-213.

Endres M, Wang ZQ, Namura S, Waeber C and Moskowitz MA, 1997. Ischemic brain injury is mediated by the activation of poly(ADP-ribose)polymerase. Journal of Cerebral Blood Flow and Metabolism 17, 1143-1151.

Engler H and Stefanski V, 2003. Social stress and T cell maturation in male rats: transient and persistent alterations in thymic function. Psychoneuroendocrinology 28, 951-969.

Fletcher AL, Lowen TE, Sakkal S, Reiseger JJ, Hammett MV, Seach N, Scott HS, Boyd RL and Chidgey AP, 2009. Ablation and regeneration of tolerance-inducing medullary thymic epithelial cells after cyclosporine, cyclophosphamide, and dexamethasone treatment. Journal of Immunology 183, 823-831.

Frohman EM, Racke MK and Raine CS, 2006. Medical progress: Multiple sclerosis - The plaque and its pathogenesis. New England Journal of Medicine 354, 942-955.

Ghafourifar P, Mousavizadeh K, Parihar MS, Nazarewicz RR, Parihar A and Zenebe WJ, 2008. Mitochondria in multiple sclerosis. Frontiers in Bioscience 13, 3116-3126.

Gray D, Seach N, Ueno T, Milton M, Liston A, Lew A, Goodnow C and Boyd RL, 2006. Developmental kinetics, turnover, and stimulatory capacity of thymic epithelial cells. Blood 108, 3777-3785.

Gruver AL and Sempowski GD, 2008. Cytokines, leptin, and stress-induced thymic atrophy. Journal of Leukocyte Biology 84, 915-923.

Gudi V, Moharregh-Khiabani D, Skripuletz T, Koutsoudaki PN, Kotsiari A, Skuljec J, Trebst C and Stangel M, 2009. Regional differences between grey and white matter in cuprizone induced demyelination. Brain Research 1283, 127-138.

Ha HC and Snyder SH, 2000. Poly(ADP-ribose) polymerase-1 in the nervous system. Neurobiology of Disease 7, 225-239.

Harris NG, Jones HC and Williams SCR, 1992. MR Imaging for measurements of ventricles and cerebral-cortex in postnatal rats (H-Tx strain) with progressive inherited hydrocephalus. Experimental Neurology 118, 1-6.

Hassa PO, Buerki C, Lombardi C, Imhof R and Hottiger MO, 2003. Transcriptional coactivation of nuclear factor-kappa B-dependent gene expression by p300 is regulated by poly(ADP)-ribose polymerase-1. Journal of Biological Chemistry 278, 45145-45153.

Hick RW, Gruver AL, Ventevogel MS, Haynes BF and Sempowski GD, 2006. Leptin selectively augments thymopoiesis in leptin deficiency and lipopolysaccharide-induced thymic atrophy. Journal of Immunology 177, 169-176.

Hiremath MM, Saito Y, Knapp GW, Ting JPY, Suzuki K and Matsushima GK, 1998. Microglial/macrophage accumulation during cuprizone-induced demyelination in C57BL/6 mice. Journal of Neuroimmunology 92, 38-49.

Hong SJ, Dawson TM and Dawson VL, 2004. Nuclear and mitochondrial conversations in cell death: PARP-1 and AIF signaling. Trends in Pharmacological Sciences 25, 259-264.

Hopkins RG and Failla ML, 1995. Chronic intake of a marginally low copper diet impairs in-vitro activities of lymphocytes and neutrophils from male-rats despite minimal impact on conventional indicators of copper status. Journal of Nutrition 125, 2658-2668.

Hopkins RG and Failla ML, 1999. Transcriptional regulation of interleukin-2 gene expression is impaired by copper deficiency in Jurkat human T lymphocytes. Journal of Nutrition 129, 596-601.

Hoppel CL and Tandler B, 1973. Biochemical effects of cuprizone on mouse liver and heart mitochondria. Biochemical Pharmacology 22, 2311-2318.

Huby RDJ, Hicks R and Goff LK, 1995. Kinetics of thymocyte subset development and selection revealed by Cyclosporine-A treatment. Developmental Immunology 4, 117-126.

Jagtap P and Szabo C, 2005. Poly(ADP-ribose) polymerase and the therapeutic effects of its inhibitors. Nature Reviews Drug Discovery 4, 421-440.

Jana A and Pahan K, 2007. Oxidative stress kills human primary oligodendrocytes via neutral sphingomyelinase: Implications for multiple sclerosis. Journal of Neuroimmune Pharmacology 2, 184-193.

Jurevics H, Largent C, Hostettler J, Sammond DW, Matsushima GK, Kleindienst A, Toews AD and Morell P, 2002. Alterations in metabolism and gene expression in brain regions during cuprizone-induced demyelination and remyelination. Journal of Neurochemistry 82, 126-136.

Jurewicz A, Matysiak M, Tybor K, Kilianek L, Raine CS and Selmaj K, 2005. Tumour necrosis factor-induced death of adult human oligodendrocytes is mediated by apoptosis inducing factor. Brain 128, 2675-2688.

Juurlink BHJ, 1997. Response of glial cells to ischemia: Roles of reactive oxygen species and glutathione. Neuroscience and Biobehavioral Reviews 21, 151-166.

Juurlink BHJ, Thorburne SK and Hertz L, 1998. Peroxide-scavenging deficit underlies oligodendrocyte susceptibility to oxidative stress. Glia 22, 371-378.

Kalman B, Laitinen K and Komoly S, 2007. The involvement of mitochondria in the pathogenesis of multiple sclerosis. Journal of Neuroimmunology 188, 1-12.

Karbowski M, Kurono C, Wozniak M, Ostrowski M, Teranishi M, Nishizawa Y, Usukura J, Soji T and Wakabayashi T, 1999. Free radical-induced megamitochondria formation and apoptosis. Free Radical Biology and Medicine 26, 396-409.

Kauppinen TM, Chin WY, Suh SW, Wiggins AK, Huang EJ and Swanson RA, 2006. Direct phosphorylation and regulation of poly(ADP-ribose) polymerase-1 by extracellular signal-regulated kinases 1/2. Proceedings of the National Academy of Sciences of the United States of America 103, 7136-7141.

Kauppinen TM and Swanson RA, 2007. The role of poly(ADP-ribose) polymerase-1 in CNS disease. Neuroscience 145, 1267-1272.

Kesterson JW and Carlton WW, 1970. Aqueductal stenosis as the cause of hydrocephalus in mice fed the substituted hydrazine, cuprizone. Experimental and Molecular Pathology 13, 281-294.

Kim NH, Kim K, Park WS, Son HS and Bae Y, 2007. PKB/Akt inhibits ceramide-induced apoptosis in neuroblastoma cells by blocking apoptosis-inducing factor (AIF) translocation. Journal of Cellular Biochemistry 102, 1160-1170.

Kioukia-Fougia N, Antoniou K, Bekris S, Liapi C, Christofidis I and Papadopoulou-Daifoti Z, 2002. The effects of stress exposure on the hypothalamic-pituitary-adrenal axis, thymus, thyroid hormones and glucose levels. Progress in Neuro-Psychopharmacology & Biological Psychiatry 26, 823-830.

Klug DB, Carter C, Gimenez-Conti IB and Richie ER, 2002. Thymocyte-independent and thymocyte-dependent phases of epithelial patterning in the fetal thymus. Journal of Immunology 169, 2842-2845.

Koch-Henriksen N and Sorensen PS, 2010. The changing demographic pattern of multiple sclerosis epidemiology. Lancet Neurology 9, 520-532.

Koller LD, Mulhern SA, Frankel NC, Steven MG and Williams JR, 1987. Immune dysfunction in rats fed a diet deficient in copper. American Journal of Clinical Nutrition 45, 997-1006.

Kondo A, Nakano T and Suzuki K, 1987. Blood-brain-barrier permeability to horseradish-peroxidase in twitcher and cuprizone-intoxicated mice. Brain Research 425, 186-190.

Kyewski B and Klein L, 2006. A central role for central tolerance. Annual Review of Immunology 24, 571-606.

LaPlaca MC, Zhang J, Raghupathi R, Li JH, Smith F, Bareyre FM, Snyder SH, Graham DI and McIntosh TK, 2001. Pharmacologic inhibition of poly(ADP-ribose) polymerase is neuroprotective following traumatic brain injury in rats. Journal of Neurotrauma 18, 369-376.

Lassmann H, Bruck W and Lucchinetti CF, 2007. The immunopathology of multiple sclerosis: An overview. Brain Pathology 17, 210-218.

Lorenzo HK and Susin SA, 2004. Mitochondrial effectors in caspase-independent cell death. Febs Letters 557, 14-20.

Lucchinetti C, Bruck W, Parisi J, Scheithauer B, Rodriguez M and Lassmann H, 2000. Heterogeneity of multiple sclerosis lesions: Implications for the pathogenesis of demyelination. Annals of Neurology 47, 707-717.

Ludwin SK, 1997. The pathobiology of the oligodendrocyte. Journal of Neuropathology and Experimental Neurology 56, 111-124.

Lukasewycz OA and Prohaska JR, 1990. The immune-response in copper deficiency. Annals of the New York Academy of Sciences 587, 147-159.

Lynch HE, Goldberg GL, Chidgey A, Van den Brink MRM, Boyd R and Sempowski GD, 2009. Thymic involution and immune reconstitution. Trends in Immunology 30, 366-373.

Mahad D, Ziabreva I, Lassmann H and Turnbull D, 2008. Mitochondrial defects in acute multiple sclerosis lesions. Brain 131, 1722-1735.

Malek TR and Castro I, 2010. Interleukin-2 receptor signaling: at the interface between tolerance and immunity. Immunity 33, 153-165.

Mandir AS, Poitras MF, Berliner AR, Herring WJ, Guastella DB, Feldman A, Poirier GG, Wang ZQ, Dawson TM and Dawson VL, 2000. NMDA but not non-NMDA excitotoxicity is mediated by poly(ADP-ribose) polymerase. Journal of Neuroscience 20, 8005-8011.

Matsushima GK and Morell P, 2001. The neurotoxicant, cuprizone, as a model to study demyelination and remyelination in the central nervous system. Brain Pathology 11, 107-116.

Mattson MP, 2005. NF-kappa B in the survival and plasticity of neurons. Neurochemical Research 30, 883-893.

Mclaurin J and Yong VW, 1995. Oligodendrocytes and Myelin. Neurologic Clinics 13, 23-49.

McTigue DM and Tripathi RB, 2008. The life, death, and replacement of oligodendrocytes in the adult CNS. Journal of Neurochemistry 107, 1-19.

Merkler D, Boretius S, Stadelmann C, Ernsting T, Michaelis T, Frahm J and Bruck W, 2005. Multicontrast MRI of remyelination in the central nervous system. NMR in Biomedicine 18, 395-403.

Miller SD, Vanderlugt CL, Begolka WS, Pao W, Yauch RL, Neville KL, KatzLevy Y, Carrizosa A and Kim BS, 1997. Persistent infection with Theiler's virus leads to CNS autoimmunity via epitope spreading. Nature Medicine 3, 1133-1136.

Nag S, Manias JL and Stewart DJ, 2009. Pathology and new players in the pathogenesis of brain edema. Acta Neuropathologica 118, 197-217.

Naismith RT and Cross AH, 2005. Multiple sclerosis and black holes - Connecting the pixels. Archives of Neurology 62, 1666-1668.

Nelson A, Bieber A and Rodriguez M, 2004. Contrasting murine models of MS. International MS journal 11, 95-99.

Noseworthy JH, Lucchinetti C, Rodriguez M and Weinshenker BG, 2000. Medical progress: Multiple sclerosis. New England Journal of Medicine 343, 938-952.

Oh SH and Kim K, 1999. Expression of interleukin-1 receptors in the later period of foetal thymic organ culture and during suspension culture of thymocytes from aged mice. Immunology and Cell Biology 77, 491-498.

Oka S, Kato J and Moss J, 2006. Identification and characterization of a mammalian 39-kDa poly(ADP-ribose) glycohydrolase. Journal of Biological Chemistry 281, 705-713.

Oliver FJ, Menissier-de Murcia J, Nacci C, Decker P, Andriantsitohaina R, Muller S, de la Rubia G, Stoclet JC and de Murcia G, 1999. Resistance to endotoxic shock as a consequence of defective NF-kappa B activation in poly (ADP-ribose) polymerase-1 deficient mice. Embo Journal 18, 4446-4454.

Pang Y, Zheng BY, Fan LW, Rhodes PG and Cai Z, 2007. IGF-1 protects oligodendrocyte progenitors against TNF alpha-induced damage by activation of PI3K/Akt and interruption of the mitochondrial apoptotic pathway. Glia 55, 1099-1107.

Parcellier A, Tintignac LA, Zhuravleva E and Hemmings BA, 2008. PKB and the mitochondria: AKTing on apoptosis. Cellular Signalling 20, 21-30.

Pardridge WM, 2007. Blood-brain barrier delivery. Drug Discovery Today 12, 54-61.

Park HS, Kim MS, Huh SH, Park JH, Chung JK, Kang SS and Choi EJ, 2002. Akt (protein kinase B) negatively regulates SEK1 by means of protein phosphorylation. Journal of Biological Chemistry 277, 2573-2578.

Pasquini LA, Calatayud CA, Una ALB, Millet V, Pasquini JM and Soto EF, 2007. The neurotoxic effect of cuprizone on oligodendrocytes depends on the presence of pro-inflammatory cytokines secreted by microglia. Neurochemical Research 32, 279-292.

Petrie HT and Zuniga-Pflucker JC, 2007. Zoned out: Functional mapping of stromal signaling microenvironments in the thymus. Annual Review of Immunology 25, 649-679.

Pott F, Gingele S, Clarner T, Dang J, Baumgartner W, Beyer C and Kipp M, 2009. Cuprizone effect on myelination, astrogliosis and microglia attraction in the mouse basal ganglia. Brain Research 1305, 137-149.

Prohaska JR, Downing SW and Lukasewycz OA, 1983. Chronic dietary copper deficiency alters biochemical and morphological properties of mouse lymphoid-tissues. Journal of Nutrition 113, 1583-1590.

Remington LT, Babcock AA, Zehntner SP and Owens T, 2007. Microglial recruitment, activation, and proliferation in response to primary demyelination. American Journal of Pathology 170, 1713-1724.

Ryan JA, Brunelle JK and Letai A, 2010. Heightened mitochondrial priming is the basis for apoptotic hypersensitivity of CD4(+) CD8(+) thymocytes. Proceedings of the National Academy of Sciences of the United States of America 107, 12895-12900.

Savino W, Dardenne M, Velloso LA and Silva-Barbosa SD, 2007. The thymus is a common target in malnutrition and infection. British Journal of Nutrition 98, S11-S16.

Schreiber V, Dantzer F, Ame JC and de Murcia G, 2006. Poly(ADP-ribose): novel functions for an old molecule. Nature Reviews Molecular Cell Biology 7, 517-528.

Schuurman HJ, Kuper CF and Vos JG, 1994. Histopathology of the immune-system as a tool to assess immunotoxicity. Toxicology 86, 187-212.

Scott GS, Kean RB, Mikheeva T, Fabis MJ, Mabley JG, Szabo C and Hooper DC, 2004. The therapeutic effects of PJ34 [N-(6-oxo-5,6dihydrophenanthridin-2-yl)-N,N-dimethylacetamide.HCl], a selective inhibitor of poly(ADP-ribose) polymerase, in experimental allergic encephalomyelitis are associated with immunomodulation. Journal of Pharmacology and Experimental Therapeutics 310, 1053-1061.

Segal BA, 2003. Experimental autoimmune encephalo myelitis: Cytokines, effector T cells, and antigen-presenting cells in a prototypical Th1-mediated autoimmune disease. Current Allergy and Asthma Reports 3, 86-93.

Sempowski GD, Gooding ME, Liao HX, Le PT and Haynes BF, 2002. T cell receptor excision circle assessment of thymopoiesis in aging mice. Molecular Immunology 38, 841-848.

Sidman, RL, 1971. Atlas of the mouse brain and spinal cord. Cambridge, Harvard University Press.

Skripuletz T, Bussmann JH, Gudi V, Koutsoudaki PN, Pul R, Moharregh-Khiabani D, Lindner M and Stangel M, 2010. Cerebellar cortical demyelination in the murine cuprizone model. Brain Pathology 20, 301-312.

Smith KJ and Lassmann H, 2002. The role of nitric oxide in multiple sclerosis. Lancet Neurology 1, 232-241.

Stepkowski S, 2000. Molecular targets for existing and novel immunosuppressive drugs. Expert reviews in molecular medicine 2, 1-23.

Susin SA, Lorenzo HK, Zamzami N, Marzo I, Snow BE, Brothers GM, Mangion J, Jacotot E, Costantini P, Loeffler M, Larochette N, Goodlett DR, Aebersold R, Siderovski DP, Penninger JM and Kroemer G, 1999. Molecular characterization of mitochondrial apoptosis-inducing factor. Nature 397, 441-446.

Suzuki K and Kikkawa Y, 1969. Status spongiosus of CNS and hepatic changes induced by cuprizone (biscyclohexanone oxalyldihydrazone). American Journal of Pathology 54, 307-325.

Suzuki K, 1969. Giant hepatic mitochondria: production in mice fed with cuprizone. Science 163, 81-82.

Tapodi A, Debreceni B, Hanto K, Bognar Z, Wittmann I, Gallyas F, Varbiro G and Sumegi B, 2005. Pivotal role of Akt activation in mitochondrial protection and cell survival by poly(ADP-ribose) polymerase-1 inhibition in oxidative stress. Journal of Biological Chemistry 280, 35767-35775.

Thorburne SK and Juurlink BHJ, 1996. Low glutathione and high iron govern the susceptibility of oligodendroglial precursors to oxidative stress. Journal of Neurochemistry 67, 1014-1022.

Todorich B, Pasquini JM, Garcia CI, Paez PM and Connor JR, 2009. Oligodendrocytes and myelination: The role of iron. Glia 57, 467-478.

Turrens JF, 2003. Mitochondrial formation of reactive oxygen species. Journal of Physiology 552, 335-344.

Urdahl KB, Pardoll DM and Jenkins MK, 1994. Cyclosporine-A inhibits positive selection and delays negative selection in alpha-beta TCR transgenic mice. Journal of Immunology 152, 2853-2859.

van Ewijk W, Hollander G, Terhorst C and Wang BP, 2000. Stepwise development of thymic microenvironments in vivo is regulated by thymocyte subsets. Development 127, 1583-1591.

Venturini G, 1973. Enzymic activities and sodium, potassium and copper concentrations in mouse brain and liver after cuprizone treatment *in vivo*. Journal of Neurochemistry 21, 1147-1151.

Veres B, Gallyas F, Varbiro G, Berente Z, Osz E, Szekeres G, Szabo C and Sumegi B, 2003. Decrease of the inflammatory response and induction of the Akt/protein kinase B pathway by poly-(ADP-ribose) polymerase 1 inhibitor in endotoxin-induced septic shock. Biochemical Pharmacology 65, 1373-1382.

Veres B, Radnai B, Gallyas F, Varbiro G, Berente Z, Osz E and Sumegi B, 2004. Regulation of kinase cascades and transcription factors by a poly(ADP-ribose) polymerase-1 inhibitor, 4-hydroxyquinazoline, in lipopolysaccharide-induced inflammation in mice. Journal of Pharmacology and Experimental Therapeutics 310, 247-255.

Veto S, Acs P, Bauer J, Lassmann H, Berente Z, Setalo G, Borgulya G, Sumegi B, Komoly S, Gallyas F and Illes Z, 2010. Inhibiting poly(ADP-ribose) polymerase: a potential therapy against oligodendrocyte death. Brain 133, 822-834.

Virag L and Szabo C, 2002. The therapeutic potential of poly(ADP-ribose) polymerase inhibitors. Pharmacological Reviews 54, 375-429.

Wang SD, Huang KJ, Lin YS and Lei HY, 1994. Sepsis-induced apoptosis of the thymocytes in mice. Journal of Immunology 152, 5014-5021.

Xu Y, Huang S, Liu ZG and Han JH, 2006. Poly(ADP-ribose) polymerase-1 signaling to mitochondria in necrotic cell death requires RIP1/TRAF2-mediated JNK1 activation. Journal of Biological Chemistry 281, 8788-8795.

Yoon SO, Casaccia-Bonnefil P, Carter B and Chao MV, 1998. Competitive signaling between TrkA and p75 nerve growth factor receptors determines cell survival. Journal of Neuroscience 18, 3273-3281.

Yu SW, Andrabi SA, Wang H, Kim NS, Poirier GG, Dawson TM and Dawson VL, 2006. Apoptosis-inducing factor mediates poly(ADP-ribose) (PAR) polymer-induced cell death. Proceedings of the National Academy of Sciences of the United States of America 103, 18314-18319.

Yu SW, Wang HM, Poitras MF, Coombs C, Bowers WJ, Federoff HJ, Poirier GG, Dawson TM and Dawson VL, 2002. Mediation of poly(ADP-ribose) polymerase-1-dependent cell death by apoptosis-inducing factor. Science 297, 259-263.

Zhang J, Lautar S, Huang S, Ramsey C, Cheung A and Li JH, 2000. GPI 6150 prevents H2O2 cytotoxicity by inhibiting poly(ADP-ribose) polymerase. Biochemical and Biophysical Research Communications 278, 590-598.

Zuniga-Pflucker JC, 2004. T-cell development made simple. Nature Reviews Immunology 4, 67-72.

## 9. PUBLICATIONS AND PRESENTATIONS

**Publications supporting the dissertation:**

Veto S*, Acs P*, Bauer J, Lassmann H, Berente Z, Setalo G Jr., Borgulya G, Sumegi B, Komoly S, Gallyas F Jr, Illes Z. Inhibiting poly(ADP-ribose) polymerase: a potential therapy against oligodendrocyte death. Brain, 2010, 133:822-834 IF:9.49
**SV and PA contributed equally*

Manuscript in preparation: New aspects of the degenerative demyelination model – acute thymic atrophy induced by cuprizone.

**Other publications:**

Clemens B, Bank J, Piros P, Bessenyei M, Veto S, Toth M, Kondakor I. Three-dimensional localization of abnormal EEG activity in migraine: a low resolution electromagnetic tomography (LORETA) study of migraine patients in the pain-free interval. Brain Topography, 2008; 21:36-42 IF:1.179

**Patent**

Pharmaceutical combination product for the treatment of degenerative neurological diseases
Completed Hungarian application No.: P0800414
PCT/HU2009/000055
Priority date: 2008. 07. 04.

**Citable abstracts, posters and oral presentations supporting the dissertation:**

**Abstracts:**

Veto S, Acs P, Bauer J, Lassmann H, Berente Z, Sumegi B, Komoly S, Gallyas F Jr, Illes Z, 2010. Inhibiting poly(ADP-ribose) polymerase: a potential therapy against oligodendrocyte death in multiple sclerosis. Clinical Immunology 135: S30-S30. (IF: 3.863)

Veto S, Acs P, Bauer J, Lassmann H, Berente Z, Sumegi B, Komoly S, Gallyas F Jr, Illes Z, 2010. Poly(ADP-ribose) polymerase (PARP) is activated in multiple sclerosis pattern III lesions and its inhibition prevents experimental demyelination and oligodendrocyte death. Journal of Neuroimmunology 222:16-16 (IF: 2.841)

Veto S, Acs P, Bauer J, Lassmann H, Berente Z, Sumegi B, Komoly S, Gallyas F Jr, Illes Z, 2009. Poly(ADP-ribose) polymerase (PARP) is activated in multiple sclerosis pattern III lesions and its inhibition prevents experimental demyelination and oligodendrocyte death. Journal of the Neurological Sciences 285: S105-S106 Suppl. 1 (IF: 2.324)

Veto S, Acs P, Bauer J, Lassmann H, Berente Z, Sumegi B, Komoly S, Gallyas F Jr, Illes Z, 2009. Poly(ADP-ribose) polymerase is activated in multiple sclerosis pattern III lesions and its inhibition prevents experimental demyelination and oligodendrocyte death. Multiple Sclerosis 15: S88-S88 (IF: 3.312)

Veto S, Acs P, Tapodi A, Lendvai Z, Komoly S, Illes Z, Gallyas F, 2008. Poly(ADP)ribose polymerase inhibitor modifies the activities of various kinase cascades in the cuprizone-induced demyelination model. Multiple Sclerosis 14: S81-S81 (IF: 3.312)

Veto S, Acs P, Dolowschiak T, Doppler H, Kanizsai A, Berente Z, ifj Gallyas F, 2007. Cuprizone hatása a mitogén aktiválta protein kináz (MAPK) rendszerekre a corpus callosumban. Folia Hepatologica 11: S40-S40

Veto S, Acs P, Dolowschiak T, Lendvai Z, Gallyas F, Komoly S, Berente Z, 2007. In vivo MRI follow-up of cuprizone-induced CNS changes. Multiple Sclerosis 13: S255-S255 (IF: 3.260)

Veto S, Acs P, Berente Z, Szabo A, ifj. Gallyas F, Komoly S, 2006. 4-hydroxiquinazoline hatása a cuprizone indukálta központi idegrendszeri elváltozásokra. Biokémia 30:80-81

**Oral presentations:**
Ifj. Gallyas F, Berente Z, Veto S**,** Acs P, Komoly S, Sumegi B, Illes Z. Non-invazív MRI módszer használata sclerosis multiplex degeneratív állatmodelljében: PARP gátlás, mint új terápiás lehetőség?
MBKE Gyógyszerbiokémiai Szakosztály munkaértekezlete, May 17-19, 2010 Balatonőszöd, Hungary

Veto S, Acs P, Berente Z, Lendvai Z, Komoly S, Sumegi B, Illes Z, Gallyas F Jr. Inhibition of poly(ADP)ribose polymerase prevents cuprizone-induced experimental demyelination in a degenerative murine model of multiple sclerosis.
Biológus doktoranduszok konferenciája, November 12-13, 2009, Pecs, **3rd place**

Veto S, Acs P, Bauer J, Lassmann H, Berente Z, Sumegi B, Komoly S, Gallyas F Jr, Illes Z. Poly(ADP)ribose polymerase (PARP) is activated in multiple sclerosis pattern III lesions and its inhibition prevents experimental demyelination.
19th World Congress of Neurology, October 24-30, 2009, Bangkok, Thailand

Veto S, Acs P, Berente Z, Lendvai Z, Komoly S, Illes Z, ifj. Gallyas F. A poli(ADP-ribóz)-polimeráz enzim gátlása a mitokondrium integritásának megőrzésén keresztül véd a cuprizone indukálta demyelinizáció ellen a sclerosis multiplex egy állatmodelljében.
Magyar Élettani Társaság LXXIII. Vándorgyűlése, August 27-29, 2009, Budapest, Hungary, **Merck price**

Illes Z, Veto S**,** Acs P, Lassmann H, Sumegi B, Komoly S, ifj. Gallyas F. PARP gátlás védő hatása a sclerosis multiplex (III. típus) állatmodelljében.
39. Membrán-Transzport Konferencia, May 19-22, 2009, Sümeg, Hungary

Veto S, Acs P, Dolowschiak T, Doppler H, Kanizsai A, Berente Z, ifj. Gallyas F. Cuprizone hatása a mitogén aktiválta protein kináz (MAPK) rendszerekre a corpus callosumban
Magyar Szabadgyök Kutató Társaság IV. Konferenciája, October 11-13, 2007, Pécs, Hungary

**Posters:**

Veto S, Acs P, Bauer J, Lassmann H, Berente Z, Setalo G Jr, Sümegi B, Komoly S, Gallyas F Jr, Illes Z. Poli(ADP-ribóz) polimeráz (PARP) gátlás: az oligodendrocyta pusztulás és a demyelinisatio potenciális terápiája.
Magyar Immunológiai Társaság 39. Vándorgyűlése, November 3-5, 2010, Szeged, Hungary

Veto S, Acs P, Bauer J, Lassmann H, Berente Z, Setalo G Jr, Sumegi B, Komoly S, Gallyas F Jr, Illes Z. Inhibiting poly(ADP-ribose) polymerase (PARP): a potential therapy against oligodendrocyte death and demyelination in multiple sclerosis.
14th Congress of the Europian Federation of Neurological Societies, September 25-28, 2010, Geneva, Switzerland

Veto S**,** Palinkas L, Fonai F, Lendvai Z, Balogh P, Illes Z, Gallyas F Jr. Cuprizone induces acute thymic involution which can be prevented by PARP inhibition. 40. Membrán-Transzport Konferencia, May 18-21, 2010, Sümeg, Hungary.

Veto S, Acs P, J. Bauer J, H. Lassmann, Z. Berente, B. Sumegi, S. Komoly, F. Gallyas Jr, Z. Illes. Poly(ADP-ribose) polymerase is activated in multiple sclerosis pattern III lesions and its inhibition prevents experimental demyelination and oligodendrocyte death.
25th Congress of the European Committee for Treatment and Reasearch in Multiple Sclerosis, September 9-12, 2009, Düsseldorf, Germany **nominated for best poster award**

Veto S, Acs P, Berente Z, Doppler H, Kanizsai A, Lendvai Z, Komoly S, Illes Z, Gallyas F Jr. Inhibition of poly(ADP)ribose polymerase protects against cuprizone-induced demyelination by preserving mitochondrial integrity in a degenerative murine model of multiple sclerosis.
12th Meeting of the Hungarian Neuroscience Society, 22-24 January, 2009, Budapest, Hungary **best poster award**

Veto S, Acs P, Tapodi A, Lendvai Z, Komoly S, Illes Z, Gallyas F Jr. Poly(ADP)ribose polymerase inhibitor modifies the activities of various kinase cascades in the cuprizone induced demyelination model.
World Congress on Treatment and Research in Multiple Sclerosis. September 17-20, 2008, Montreal, Canada

Veto S, Palinkas L, Lendvai Z, Balogh P, Illes Z, ifj. Gallyas F. Az immunrendszer változásai a cuprizone kiváltotta demielinizációs modellben.
38. Membrán-Transzport Konferencia, May 20-23, 2008, Sümeg, Hungary

Veto S, Acs P, Dolowschiak T, Lendvai Z, Gallyas F Jr., Komoly S, Berente Z. In vivo MRI follow-up of cuprizone induced CNS changes.
23rd Congress of the European Committee for Treatment and Research of Multiple Sclerosis (ECTRIMS) and the 12th Conference of Rehabilitation in Multiple Sclerosis (RIMS), October 11–14, 2007, Prague, Czech Republic

Veto S, Dolowschiak T, Kanizsai A, Doppler H, Acs P, ifj. Gallyas F, Komoly S, Berente Z. Cuprizone indukálta központi idegrendszeri elváltozások *in vivo* követése MRI segítségével.
37. Membrán-Transzport Konferencia, May 22-25, 2007, Sümeg, Hungary

Veto S, Acs P, Berente Z, Szabo A, ifj. Gallyas F, Komoly S. 4-hydroxiquinazoline hatása a cuprizone indukálta központi idegrendszeri elváltozásokra.
A Magyar Biokémiai Egyesület 2006. évi Vándorgyűlése, August 30 – September 2, 2006, Pécs, Hungary

**Other citable abstracts, posters and oral presentations**

**Abstracts:**
Radnai B, Tucsek Z, Hocsak E, Veto S, Nemeth V, Bognar E, Grasz D, Berente Z, ifj. Gallyas F, Sumegi B, 2006. A ferulaldehid hatása az LPS indukálta endotoxikus sokkra egerekben. Biokémia 30: 63-63

Solti I, Bognar Z, Nemeth V, Bognar E, Veto S, Hocsak E, N Kiss G, Szanto A, Varbiro G, Sumegi B, 2006. Taxol hatása a mitokondriumra és a szabadgyökképződésre. Biokémia 30:81-82

Nemeth V, Montsko G, Solti I, Veto S, Tucsek Z, Hocsak E, Mark L, 2006. Komplex biológiai minták GSH-tartalmának meghatározása ioncsapdás tömegspektrometria segítségével. Biokémia 30:81-81

Radnai B, Veres B, Hanto K, Jakus P, Varbiro G, Bognar Z, Tapodi A, Veto S, Sumegi B, 2005. The effect of a novel PARP inhibitor HO-3089 on the LPS stimulated RAW 264,7 murine macrophage cells. FEBS Journal 272:313-313 Suppl.1

Kondakor I, Bank J, Bessenyei M, Piros P, Toth M, Veto S, Clemens B, 2005. Kezeltlen migrénes betegek EEG háttértevékenységének elemzése agyi elektromágneses tomográfia (LORETA) segítségével. Cephalalgia Hungarica 13:11-12

**Oral presentations:**
Sumegi B, Veto S**,** Tucsek Z, Solti I, Hocsak E, Bognar E, Szabo A, Gallyas F Jr. PARP and inflammatory and kinase pathway: relevance for endotoxic shock.
Semmelweis Symposium, 29-31st October 2006, Budapest, Hungary

Radnai B, Tucsek Z, Hocsak E, Veto S, Nemeth V, Bognar E, Grasz D, Berente Z, ifj. Gallyas F, Sumegi B. A ferulaldehid hatása az LPS indukálta endotoxikus sokkra egerekben.
A Magyar Biokémiai Egyesület 2006. évi Vándorgyűlése, August 30 - September 2, 2006, Pécs, Hungary

Kondakor I, Bank J, Bessenyei M, Piros P, Toth M, Veto S**,** Clemens B. Kezeletlen migrénes betegek EEG háttértevékenységének elemzése agyi elektromágneses tomográfia (LORETA) segítségével.

A Magyar Fejfájás Társaság XII. Kongresszusa, April 29-30, 2005 Siófok, Hungary

**Posters:**

Montsko G, Veto S, Mark L, Boddi K, Dolowschiak T, Kanizsai A, Doppler H, Ohmacht R. Biokompatibilis fullerén oldatok analitikai és toxicologiai vizsgálata.
37. Membrán-Transzport Konferencia, May 22-25, 2007, Sümeg, Hungary

Solti I, Bognar Z, Nemeth V, Bognar E, Veto S, Hocsak E., N Kiss G, Szanto A, Varbiro G, Sumegi B. Taxol hatása a mitokondriumra és a szabadgyökképződésre.
A Magyar Biokémiai Egyesület 2006. évi Vándorgyűlése, August 30 - September 2, 2006, Pécs, Hungary

Nemeth V, Montsko G, Solti I, Veto S, Tucsek Z, Hocsak E, Mark L. Komplex biológiai minták GSH-tartalmának meghatározása ioncsapdás tömegspektrometria segítségével.
A Magyar Biokémiai Egyesület 2006. évi Vándorgyűlése, August 30 - September 2, 2006, Pécs, Hungary

Tucsek Z, Radnai B, Szabo Z, Dolowschiak T, Hocsak E, Szabo A, Solti I, Bognar E, Veto S, ifj.Gallyas F, Lorand T, Sumegi B. A PJ34 protektív hatása az IK11 indukálta oxidatív stresszben HepG2 sejtvonalon.
36. Membrán-Transzport Konferencia, May 23-26, 2006, Sümeg, Hungary

Hocsak E, Bellyei S, Szigeti A, Boronkai A, Tucsek Z, Szabo A, Veto S, Berki T, Sumegi B. A PP17B fehérje struktúrális és funkcionális vizsgálatai.
36. Membrán-Transzport Konferencia, May 23-26, 2006, Sümeg, Hungary

Szanto A, Szabo A, Bognar Z, Tapodi A, Jakus P, Veto S, Tucsek Z, Poor V, Sumegi B. Inhibition of poly-(ADP-ribose) polymerase influence the taxol induced cell death in cultured cells.
36. Membrán-Transzport Konferencia, May 23-26, 2006, Sümeg, Hungary

Veto S, Solti I, Szabo A, Tucsek Z, Nemeth V, Hocsak E, Veres B, Berente Z, Sumegi B. Involvement of Akt/protein kinase B pathway induction in the protective effect of poly-(ADP-ribose) polymerase 1 inhibition in endotoxin-induced septic shock.
36. Membrán-Transzport Konferencia, May 23-26, 2006, Sümeg, Hungary

Solti I, Bognar E, Tucsek Z, Veto S, Varbiro G, Szanto A, Sumegi B. Taxol induced mitochondrial permeability transition and free radical formation.
36. Membrán-Transzport Konferencia, May 23-26, 2006, Sümeg, Hungary

Nemeth V, Montsko G, Veto S, Bognar E, Mark L. MALDI TOF/TOF tömegspektrometria alkalmazása a jelátviteli folyamatokban jelentős kis molekulatömegű fehérjék azonosítására.
36. Membrán-Transzport Konferencia, May 23-26, 2006, Sümeg, Hungary

Radnai B, Veres B, Hanto K, Jakus P, Tapodi A, Varbiro G, Bognar Z, Veto S, Sumegi B. The effect of a novell PARP inhibitor HO-3089 on the LPS stimulated RAW 264,7 murine macrophage cells.

30th FEBS Congress and 9th IUBMB Conference, 2-7th July 2005, Budapest, Hungary

Bognar Z, ifj. Gallyas F, Radnai B, Tapodi A, Hanto K, Szabo A, Jakus P, Veto S, Bognar E, Varbiro G, Sumegi B. PARP inhibitorok hatása a Taxol indukálta sejthalálra sejkultúrákon.
Magyar Szabadgyökkutató Társaság III. Konferenciája, October 13-15, 2005, Debrecen, Hungary

Radnai B, Veres B, Hanto K, Jakus P, Tapodi A, Varbiro G, Bognar Z, Veto S, Sumegi B. Egy új PARP-gátló szer, a HO-3089 hatása az LPS stimulálta egér makrofág sejtvonalon.
XIII. Sejt- és fejlődésbiológiai napok, April 10-12, 2005, Eger, Hungary